Acta Futura 12 (2020) 9-45
DOI: 10.5281/zenodo.3747263

Acta Futura

The Path to Interstellar Flight

LUBIN, P.* AND HETTEL, W.

DEPARTMENT OF PHYSICS, UNIVERSITY OF CALIFORNIA AT SANTA BARBARA, SANTA BARBARA CA 93106 (USA)

Abstract. Large scale directed energy offers the possibility of radical transformation in a variety of areas, including the ability to achieve relativistic flight that will enable the first interstellar missions as well as rapid interplanetary transit. In addition, the same technology opens a wide mission space that allows a diverse range of options from long range beamed power to remote spacecraft and outposts to planetary defense to remote composition analysis and manipulation of asteroids, among others. Directed energy relies on photonics, which like electronics is an exponentially expanding growth area driven by diverse economic interests that allows transformational advances in space exploration and capability. In order to begin to fully exploit this capability it is important to understand not only the possibilities enabled by it, but also the technological challenges involved and to have a logical roadmap to exploit this option. This capability is both synergistic with conventional propulsion and offers a road to a future currently not possible with conventional capabilities.

1 Introduction

One of the dreams of humanity has been to travel to the stars. With the number of planets per star being approximately unity based on the latest Kepler data and with even our nearest stellar neighbor, the Alpha Centauri system, having at least one confirmed exoplanet, the possibility of reaching interstellar targets is a dream we can came begin to seriously explore. However, the ability to travel to and explore the many nearby exoplanets requires a radical change in both propulsion systems and in spacecraft design. The ability to achieve the speeds required is becoming a possibility due to recent advances in directed energy systems that allow us to remove the propulsion system and its associated mass from the spacecraft. The transformations that will come from this approach allow a radical change in capability.

One question that is often pondered in space exploration is, "Why do we want to go there?" This is a valid question and should not be dismissed as simply, "It is in the human spirit to explore."

The question is more quantitatively proposed as, "How close do we need to get to answer the questions we pose?" This at least can be quantified for a given question and set of assumptions.

For example, our atmosphere is quite opaque shortward of 330 nm and thus trying to conduct deep UV or X-Ray observations from the ground is not feasible. As a quantitative example let us suppose we bring a 10 cm diameter telescope to the nearest star to look, even if we do not land. What do we learn that a large space or ground based telescope will not "show us?" Suppose we take our 10 cm telescope to within 1 AU of the star or exoplanet. What size Earth (or near Earth) telescope would we need to be equivalent in resolution? This is simple to answer–it is just the ratio of distances. The nearest star, Proxima Centauri,

*Corresponding author. E-mail: lubin@ucsb.edu

is about 250,000 AU (4.2 ly) and thus our 10 cm telescope at Proxima C is equal in angular resolution to a $0.1 \times 250,000 = 25,000\,\mathrm{m} = 25$ km telescope. In theory, we could build such a telescope. Indeed we will see that our system discussed below when used in the "receive mode" is actually a multi-km "telescope," though not a general purpose one. Now, let's get to within 0.1 AU. The equivalent near Earth telescope, in terms of resolution, would be 250 km. This is a little harder to build. We can keep playing this game and come to the same conclusion, though on quantitative grounds, that IF we can "go there" we do learn a lot compared to "just remote sensing from the Earth or nearby." In the end it will be a question of feasibility and "cost versus benefit" and what are the secondary "spinoffs" of the technology development required to "get there."

There is a profound difference in what we have been able to do in accelerating material via chemical means versus electromagnetic means. In order to achieve relativistic flight with propellants it is necessary to have a relativistic "propulsion exhaust." It is useful to consider the energy release per unit mass as a metric for propellants. We can define an effective fractional energy release metric $\varepsilon = \Delta E/mc^2$ where ΔE is the energy released for a reactant mass m. This is an optimistic metric as it is assumes zero storage (confinement) and reaction chamber mass. With the chemical energy per molecular bond of approximately 1 eV compared to the rest mass energy equivalent of the molecule itself of billions of eV, this gives $\varepsilon < 10^{-9}$ and thus the ability to use any chemical process that is carried on the spacecraft to achieve relativistic speeds is not feasible. In order to achieve relativistic flight with any form of "propellant" carried on-board we need energy release per unit rest mass of order unity. With any chemical process this is not possible and even with nuclear fission ($\varepsilon < 10^{-4}$) and fusion ($\varepsilon < 10^{-3}$) the ability to do this is extremely limited, even if the technology to do so was feasible. The only two choices with known physics are antimatter (annihilation) engines and stand-off directed energy propulsion. Even ignoring the production costs for antimatter we are still faced with the large confinement and reaction masses needed for any realistic variant of matter annihilation engines. While nuclear fusion is often invoked as a possible solution to relativistic flight, a detailed analysis shows the relative low equivalent energy ($\varepsilon \sim 10^{-3}$) combined with the extremely large secondary masses needed (storage and reaction), force any such system to become extremely large with modest performance. For nuclear fusion, in particular, it is instructive to consider the mass of highly optimized system, such as thermonuclear weapons. The highest energy yield per unit mass is approximately 5 MT/Ton or an effective system energy release metric of $\varepsilon = \Delta E/mc^2 \sim 2 \times 10^{16}\ \mathrm{J}/(10^3\ \mathrm{kg})c^2 \sim 2 \times 10^{-4}$. Looking at systems such as Tokomaks, the efficiency is vastly less than this, though these are not optimized for mass efficiency. Annihilation engines then seem like a "logical" next step in analysis, but all known confinement options (laser, magnetic bottles, etc.) also yield low effective overall system efficiencies due to the large additional masses required. Thus annihilation engines (even if we could produce and store the required antimatter) do not appear feasible.

2 Directed Energy Approaches

A completely different approach is to "leave the propulsion system at home" by using photons from a source not on the spacecraft. In this approach no propellant is carried and the propulsion is achieved by direct transfer of the photon momentum to the spacecraft via reflection. This is an old concept and is the basis for solar sails, as one example. While solar sails cannot achieve relativistic speeds and thus are not useful for interstellar flight, laser driven sails can and are. The difficulty in using a laser driven system is the ability to produce a directed energy system that is sufficiently powerful and collimated, both of which are required. This is shown artistically in Figure 1.

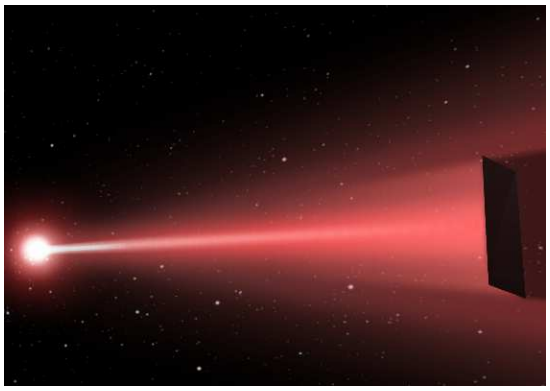

FIGURE 1. *Artistic license and rendering of a laser driven reflector. Credit: Q. Zhang – UC Santa Barbara.*

This difference in achieved speeds is dramatically illustrated if we compare beta (v/c) and gamma factors

 DOI: 10.5281/zenodo.3747263

(Figure 2). We clearly have the ability to produce highly relativistic systems, but only at the particle level. Practical systems need to be macroscopic as we do not currently have the technological means to self assemble relativistic particles into macroscopic systems. Electromagnetic acceleration is only limited by the speed of light while chemical systems are limited to the energy of chemical processes, which are typically of order 1 eV per bond or molecule. To reach relativistic speeds we would need GeV per bond equivalent, or about a billion times larger than chemical interactions.

We propose electromagnetic acceleration to achieve relativistic speeds for macroscopic objects, not by using conventional accelerators but by using light to directly couple to macroscopic objects. This concept is the simple use of a very intense light source to accelerate matter. It has the additional advantage of leaving the propulsion source behind to greatly reduce the spacecraft mass. Of course, this method has the disadvantage of reducing or eliminating (depending on the system design) maneuverability once accelerated. For many systems this is not acceptable, so hybrid systems are proposed as well as pure photon driven systems.

While photon drive is not a new concept, directed energy photonic technology has recently progressed to the point where it is possible to begin to seriously consider the construction of systems to accelerate macroscopic systems to relativistic speeds. Reaching relativistic speeds with macroscopic systems would be a watershed moment for humanity in our path to the stars.

Recent changes in directed energy, combined with miniaturized probes, allow a path to relativistic flight that was not previously possible. **These technologies also allow for a completely modular and scalable technology without "dead ends"** [1, 2]. This will allow us to take the step to interstellar exploration, enabling us to reach nearby stars in a human lifetime. We have discussed this in a series of papers which also describe the numerous additional capabilities that arise from this technology [3, 4].

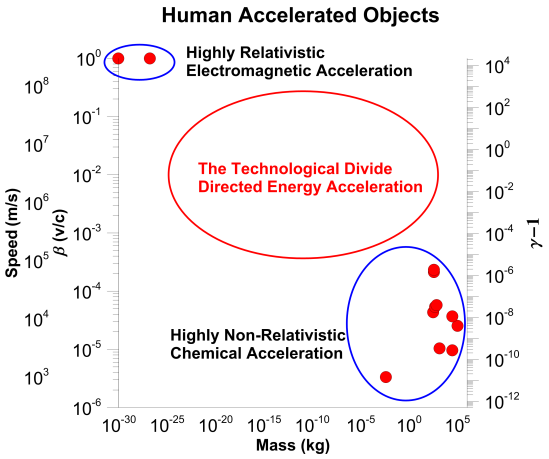

FIGURE 2. *Speed, Fractional speed of light achieved by human accelerated objects vs mass of object from subatomic to large macroscopic objects. Righthand "y" axis shows $\gamma - 1$ where γ is the relativistic "gamma factor." $\gamma - 1$ times the rest mass energy is the kinetic energy of the object.*

3 Phased Array Laser

The key to this program is the ability to build a sufficiently powerful laser photon driver with a large enough effective aperture to allow the beam to "stay on the spacecraft" long enough to propel it to high speed. For relativistic flight ($> 0.1c$), development of low mass probes is also needed. Recent developments now make both of these possible. The photon driver is a laser phased array, which eliminates the need to develop one extremely large laser and replaces it with a large number of modest laser amplifiers arranged in a MOPA (Master Oscillator Power Amplifier) configuration. Our current system uses baseline Yb amplifiers operating at 1064 nm, but this design is wavelength agnostic. The system is inherently phase lockable, as it is fed by one seed laser (see Figure 3), although maintaining phase integrity is one of the key challenges. This approach is analogous to building a supercomputer from a large number of modest processors. It also eliminates the need for large conventional optics and replaces them with an array of small low cost optical elements. As an example, on the eventual upper end, a full scale system ($\sim$100 GW) will propel a gram scale spacecraft with a **meter class reflector** (laser sail) to about $c/4$ in a **few minutes of laser illumination, allowing hundreds of launches per day or 10^5 missions per year.** Such a system would reach the distance to **Mars (1 AU) in 30 minutes, pass Voyager I in less than 3 days, pass 1,000 AU in 12 days and reach Alpha Centauri in about 20 years.** The same photon driver can also **propel a 10 kg payload to about 2.5% *c*, a 100 kg payload to about 1% *c* and a 10,000 kg payload to more than 1,000 km/s**. The system is scalable to any level of power and array size where the trade-off is between array power, array size, spacecraft mass and desired

speed. The system is also modular with identical subelements allowing for a logical build phase with critical and immediately useful milestones along the path to building increasingly capable systems. There is no upper limit to the power of the system, which allows for the investment in the core technology development to be amortized. One of the advantages of this approach is that once the photon driver is constructed it can be used on a wide variety of missions, from large mass interplanetary using beamed power to high performance ion engines to low mass interstellar probes, with all missions using the same core technology and in many cases the same laser array. This allows an enormous cost savings in the long run as this opens an essentially unlimited mission space. A range of applications is discussed in detail in our more than 50 technical papers.

The small relativistic interstellar missions are flyby missions as no current technology allows for sufficient deceleration, except for another laser array at the target, which is not feasible for the interstellar case. On the larger mass end a 1 metric ton spacecraft could be sent to Mars in about 11 days with a peak speed at midpoint of about 320 km/s, and assuming either a second laser array at Mars or a retroreflector system to reflect back the laser light from the Earth/lunar based system is then used to slow down the spacecraft. A 10 metric ton spacecraft would take about one month with a peak speed at midpoint of about 100 km/s and a 100 metric ton spacecraft would take about 4 months and reach a peak speed at midpoint of about 32 km/s. On the lower mass end, a 100 kg payload reaches Mars in 3.5 days with a peak speed of 1000 km/s, a 10 kg payload reaches Mars in one day with a peak speed of 3000 km/s, and a 1 kg payload reaches Mars in about 8 hours with a peak speed of about 10,000 km/s. Each of these systems (to Mars) would require a spacecraft reflector that is only about 15-20 meters in diameter and can be made of existing materials as the flux is modest for large payloads. Note that the reflector size for Mars missions is smaller than that used for maximum speed as Mars is relatively "close." For exploring the outer solar system, an example would be a 100 kg spacecraft with a 1 km reflector that reaches a speed of 2400 km/s at 26 AU in 37 days and achieves a limiting speed of 3400 km/s (1.1% c). Such a system (100 kg) reaches the solar gravity lens focus ($\sim$ 550 AU) in less than 1 year. **These systems are vastly faster than any currently imagined conventional propulsion system including ion engines, solar sails, e-sails, etc.** For high mass nonrelativistic solar system missions another approach that is more energy efficient is to use the laser array to beam power to the spacecraft and then photoconvert to power high I_{sp} ion engines.

3.1 Modularity and Scalability

The laser photon driver is completely modular and scalable and lends itself to mass production as all the elements are identical. There are very large economies of scale in such a system in addition to exponential photonics growth. The system has no expendables, is completely solid state and can run continuously for years. Industrial fiber lasers and amplifiers have mean time between failures (MTBF) in excess of 50,000 hrs. The revolution in solid state lighting, including up-coming laser lighting, will only further increase the performance and lower the cost. We have already achieved 43% wall plug efficiency in our lab with efficiency limited by the pump diode efficiency. New diode designs promise ever higher efficiencies and allow full system amplifier efficiencies greater than 50% in the near future. The same basic system can also be used as a phased array telescope for the receive side for laser communications, as well as for future kilometer scale telescopes for specialized applications such as spectroscopy of exoplanet atmospheres and high redshift cosmology studies (see Figure 4).

3.2 Exponential Growth in Photonics is Key

Photonics, like electronics, is an exponential growth sector in both performance and in cost reductions with "Moore's-like" characteristic doubling times in performance and "halving times" in cost of approximately 18 months. This is radically different than chemical propulsion, where performance has changed little since the dawn of the space age. This is shown clearly in the accompanying plots (Figure 5). While there is wonderful innovation in chemical propulsion, ion engines, and related technologies, the innovation and drive in photonics is vastly beyond other propulsion technologies. This is largely due to the fundamental market needs, low cost of the materials used and the ability to nanofabricate (wafer scale) the relevant components. Much more is coming in photonics and electronics in the coming decades, while performance in chemical propulsion peaked many decades ago. Of particular interest is the work in integrated III-V on Si wafer scale directed energy (DE) systems we are working on at UC Santa Bar-

 DOI: 10.5281/zenodo.3747263

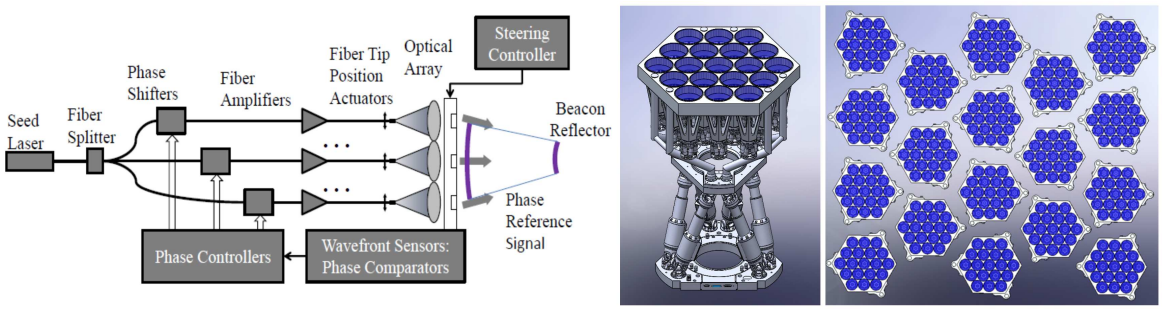

FIGURE 3. ***Left:*** *Schematic design of phased array laser photon driver. Wavefront (phase) sensing from both local and extended beacons combined with the system metrology are critical to phasing (forming) the final diffraction-limited beam.* ***Center:*** *Design of a one-meter hexagonal module with 19 optical elements, each of which is connected to a laser amplifier as in the Left figure. This panel then forms the basis for "tiling" the array. The actual number of optical elements in the module will depend on the final choice of laser amplifiers.* ***Right:*** *A portion of the array of hexagonal panels (as in the center figure) that make up the final array. The panels are as close packed as possible to minimize sidelobe power and be consistent with pointing requirements. Shown spacing allows 30 degree tilt.*

bara and many other places that could vastly lower the cost and increase the performance of the laser array.

3.3 Long Coherence Length Amplifiers

Photonic amplifiers have intrinsic minimum bandwidths B set by a variety of internal characteristics that depend on the detailed physics of the amplification process, as well as material instabilities. This bandwidth translates into a coherence length $l_{\rm coh} = c/B$ which significantly affects the system design and complexity. Long coherence length is strongly desired to eliminate the need for complex optical delay lines, where "long" is relative to the overall size (diameter) of the photon driver. For the current generation of Yb fiber amplifiers the coherence length is severely limited by the onset of stimulated Brillouin scattering (SBS) at high power levels and is often simply referred to as the SBS limit. It is caused by non-linearities in the fiber and converts the optical power into thermal acoustic phonon modes that produce an effective optical grating by changes in the fiber index of refraction, which cause severe back reflections and thus remove power from the outgoing photons and convert it into backwards propagating photons. This can not only ultimately reduce the output power but can quickly lead to amplifier destruction if there is no effective mitigation. The onset of the SBS mode can be very sudden as the power is increased and is a problem in not only high power Yb amplifiers of the type we are using now, but is also a common problem in telecommunication with Er amplifiers at 1.55 microns. For Yb amplifiers the onset in single mode fibers of the type we are using starts at power levels above about 100 watts. For power levels below this the amplifier bandwidth can be below 5 kHz, corresponding to a coherence length of about 60 km. This is more than sufficient for our need for kilometer class arrays. This is a technological limit, and solutions for increasing this SBS limit will undoubtedly come in the future. Other types of optical amplifiers are emerging that are not fiber based and these may offer lower cost and shorter wavelength options in the future. The desire for a particular power level from an amplifier is set by a number of issues, some economic and some system related. For economic reasons there is a desire to minimize the number of amplifiers, and thus increase the power per amplifier, but for reasons having to do with atmospheric perturbations and adaptive optics considerations for ground based testing and operation, we do not want the individual optical apertures, to which each amplifier is attached, to exceed about 10 cm in diameter. This is a complex trade space and one which will evolve as we learn more about the atmospheric issues during the test phase. For space based systems there are other issues having to do with the stability and economics of low areal mass diffraction limited optics.

One of the ways of mitigating the SBS limit in order to increase the power level is to artificially modulate the optical input by very rapid wavelength (offset) switching. SBS is an acoustical mode and takes some time to build up (as it is a mechanical process) and this acoustical mode causes an effective fiber grating that is very

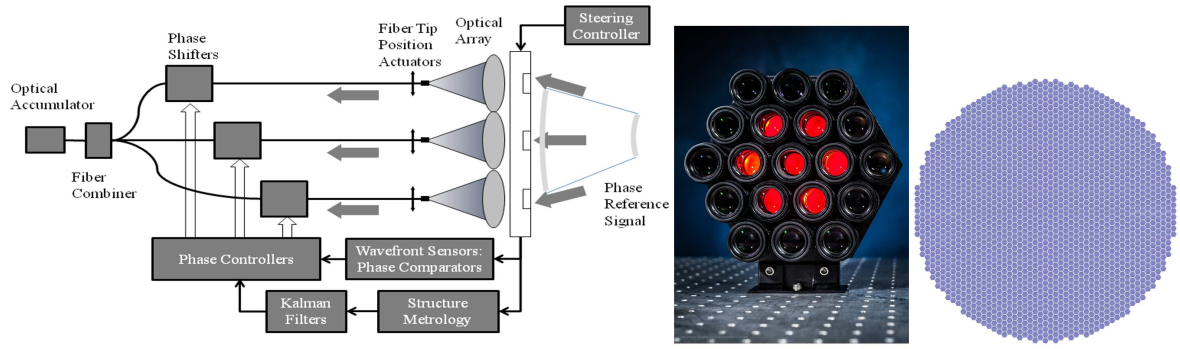

FIGURE 4. ***Left:*** *The same laser array used for propulsion can be used in reverse as a phased array telescope allowing dual use of the system for large aperture laser communications reception (needed for interstellar missions) and offers a path forward to a kilometer class telescope for many other purposes.* ***Center:*** *1/4 scale panel of phased array hexagonal module with single mode optical fibers attached.* ***Right:*** *Example of hexagonal close packed array – diameter of 50 panels.*

narrow in (reflection) bandwidth. The input wavelength modulation is found to be effective if the modulation is approximately 10 GHz/kW when in the SBS limited regime. This has currently allowed Yb amplifiers to achieve above 3 kW of power when (pseudo randomly) modulated at 30 GHz. The bottom line here is that (currently) above 100 watts the bandwidth needs to be large (10 GHz range and thus centimeter coherence length) to avoid SBS while below 100 watts the bandwidth is narrow (5-10 kHz) and thus the coherence length is very large (30-60 km). Working with high power SBS limited amplifiers with kilowatt power would be extremely difficult due to the small coherence length (cm scale) and thus requiring active optical delay lines to deal with both atmospheric perturbations and geometric path length differences from "off the array normal" angles in targeting. For this reason we are concentrating on long coherence length approaches and thus lower power non-SBS limited amplifiers, currently below 100 watts per amplifier. A related trade-off is the atmospheric limited desire to keep each sub-aperture smaller than about 10 cm. This is related to the characteristic perturbation scale (Fried length = r_0, where r_0 is the effective size of "telescope" beyond which atmospheric perturbations will limit the angular resolution). Depending on the desired laser array aperture areal power density needed for the overall mission this provides another input to this trade space. For example, if we choose 100 GW total power with a 1 km array we get an aperture areal power density of 100 kW/m^2 or 10 W/cm^2. If we want to use 100 watt narrow band (long coherence length) amplifiers we would need sub-apertures that are about 3 cm in diameter, which is less than r_0. Typical values of r_0 for "good sites" are approximately 10-20 cm at visible wavelengths depending on "seeing conditions" with r_0 varying mildly with wavelength. For example, in a Kolmogorov model of atmospheric perturbations $r_0 \propto \lambda^{6/5}$.

If we were to place this same 100 GW of power into an array that is 10 km then the aperture power density would be 1 kW/m^2 or 0.1 W/cm^2. This is about the same flux as solar illumination on a clear day at noon for a surface normal to the illumination. If we were to use the same 100 watt narrow band amplifiers as above then the sub-aperture size would be about 30 cm, which is too large for a ground based system. If we reduce the power per amplifier to 10 watts then we would have a sub aperture size of about 10 cm which is appropriate for ground use and is our current baseline. For economic reasons we also want to optimize the cost, where we trade the cost of optics versus the cost of optical amplifiers and the economics of scale for each. There are also many other approaches we are exploring that use other technologies. This will be an evolving area as we move forward. The bottom line here is we highly desire to have long coherence lengths and already have at least one path forward to do so.

3.4 Array Site Location

There are a variety of places to locate the photon driver, from the surface of the Earth, to LEO, to GEO, to Lagrange points and to the moon (see Figure 6 for an artis-

 DOI: 10.5281/zenodo.3747263

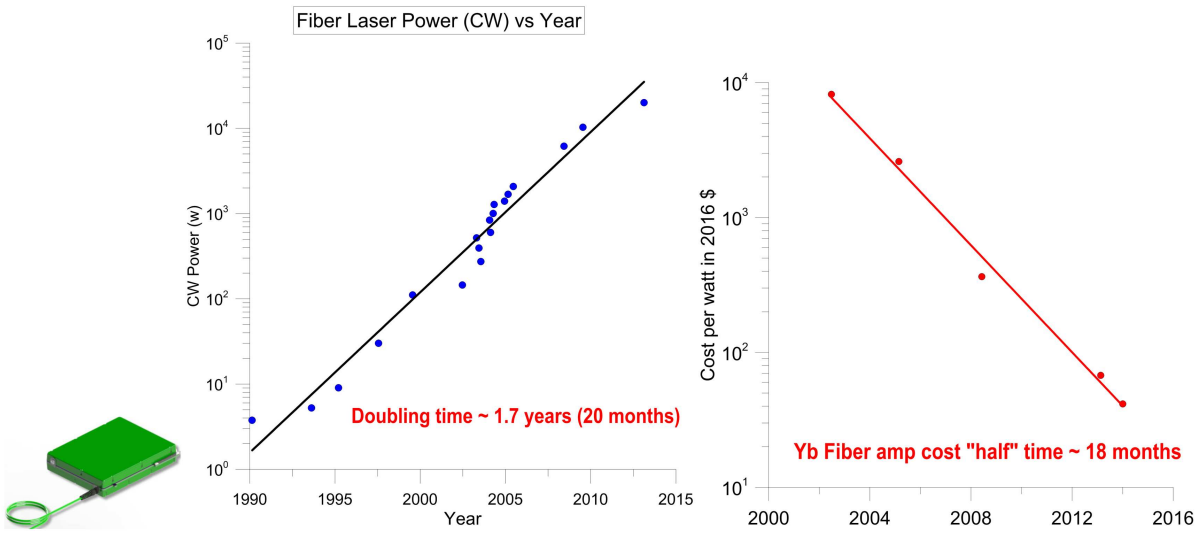

FIGURE 5. ***Left:*** *Picture of a current 1-3 kW class short wavelength Yb laser amplifier (courtesy Nufern). Our baseline is a lower power long coherence length design we have developed at UCSB. Its mass is approximately 5 kg and size is approximately that of this page. This technology is evolving rapidly but is already sufficient to begin.* ***Middle:*** *Continuous wave (CW) fiber laser power vs year over 25 years showing a "Moore's Law" like progression with a doubling time of about 20 months.* ***Right:*** *Yb fiber laser amplifiers cost/watt with an inflation index correction to bring it to 2016 dollars. Note the excellent fit to an exponential curve with a cost "halving" time of 18 months.*

tic rendition). The surface of the Earth is where the first arrays will be placed, but while the Earth's surface has both significant logistical and practical advantages, it also has complicated disadvantages. The advantages are ease of construction and much lower initial cost. The disadvantages are the atmospheric issues that must be mitigated as well as the complexity introduced in targeting of the spacecraft, especially for mid latitude sites. Sites near the poles, especially the Antarctic sites such as Dome and A, C, F, and possibly the South Pole, offer significant targeting advantages compared to mid latitude sites but also present serious siting issues and still suffer atmospheric perturbation issues. Outside the Earth, LEO sun synchronous orbits and GEO are attractive but require a much larger launch capability than we currently have, as well as the ability to build kilometer scale space structures. The moon is a particularly appealing site, especially the backside (for policy reasons), but a lunar presence would need to be built to support such a system. In the future the moon may be extremely beneficial in using the in-situ lunar resources for laser driven ablation engine rockets. With in-situ space resource utilization the lunar siting becomes particularly attractive due to its low escape speed for lunar-asteroid-Earth-Mars missions. Since the same system can be used for many other applications the costs are amortized over multiple missions [3, 4].

4 Physics and Mathematics of Photon Driven Propulsion

The nonrelativistic solution is discussed and derived in [4, 2] and the relativistic case in [5]. We summarize the nonrelativistic solution below.

We assume a laser power P_0 in the main beam (that which illuminates the sail) and a total mass (spacecraft + sail) m. Note that due to power in the side lobes the power in the main beam (on the sail) P_0 is not the same as the total optical power generated. This is accounted for below in a beam efficiency factor. The beam efficiency $\varepsilon_{\rm beam}$ (fraction of total photon power in the main beam) for a photon driver composed of a hexagonal close packed array of circular apertures is about 62%. We solve for a square or circular laser array incident on a square, circular, or spherical sail in any combination with idealized uniform reflectivity over the surface. Assume the laser array has size d and the sail has size D. For a circular array of diameter d the diffraction pattern is modified by a

DOI: 10.5281/zenodo.3747263

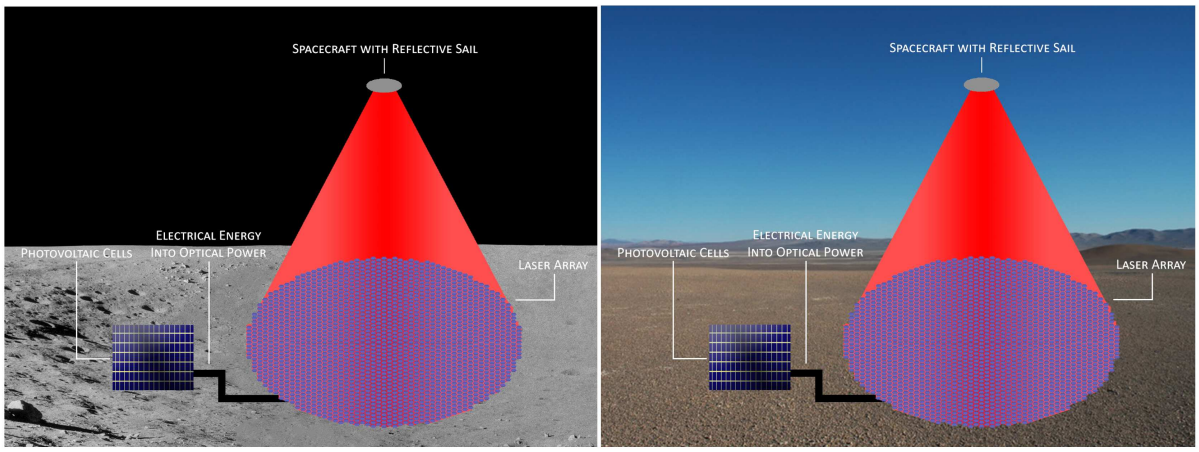

FIGURE 6. *Artistic rendition of a laser array placed on the moon (left) and on Earth (right).*

factor of α_d, where α_d is related to the first minimum of the Bessel function of the first kind J_1. In this case $\alpha \sim 1.22$. Below we parameterize the array as square ($\alpha_d = 1$) and circular ($\alpha_d = 1.22$) for generality. We allow either square or circular sails (reflectors) with surface area (to account for sail mass) $A = \xi D^2$ where $\xi = 1$ for square, $\pi/4$ for circular, and π for spherical. The speed is proportional to $\alpha_d^{-1/2}\xi^{-1/4}$ for the optimized case (sail mass = bare spacecraft mass). A circular array of the same power and size on a square sail is slower by $\alpha_d^{-1/2} = (1.22)^{-1/2} = 0.905$, or about 9.5% slower compared to a square array on a square sail. However, for a circular array on a circular sail the speed is only lower by $\alpha_d^{-1/2}\xi^{-1/4} = (1.22)^{-1/2}(\pi/4)^{-1/4} = 0.962$, or 3.8% slower, while a circular array with a spherical reflector is slower by $\alpha_d^{-1/2}\xi^{-1/4} = (1.22)^{-1/2}(\pi)^{-1/4} = 0.68$, or 32% slower. Note that in the case of a spherical reflector we may be able to use a thinner material if we inflate the reflector and hence the speed penalty may be much less than 32%. In some cases the inflated spherical reflector may actually be less massive due to the lack of required stiffeners. Note that the two terms $\alpha_d^{-1/2}$ and $\xi^{-1/4}$ are related to the array diffraction pattern and the reflector respectively.

We summarize the general relationships. Here we allow both reflection ε_r and absorption α. The parameter scaling is important to note.

$F = P_0(2\varepsilon_r + (1-\varepsilon_r)\alpha)/c$ = laser thrust on payload with laser power in the main beam P_0 with sail reflection ε_r and sail absorption coefficient α while laser spot is smaller than sail, where $\varepsilon_r = 0$ for no reflection (all absorbed with $\alpha = 1$) and 1 for complete reflection. For many cases we can assume for simplicity that $\varepsilon_r \sim 1 \rightarrow 2\varepsilon_r + (1-\varepsilon_r)\alpha \sim 2$.

$a = F/m = P_0(2\varepsilon_r + (1-\varepsilon_r)\alpha)/mc$ = acceleration.

$m = m_{\rm sail} + m_0$ = total mass of sail + base payload mass m_0.

$m_{\rm sail} = \xi D^2 h\rho$ where D = sail size, h = sail thickness, ρ = sail density, $\xi = 1$ (square), $\xi = \pi/4$ (circular), $\xi = \pi$ (sphere).

$$D(m) = \sqrt{m_{\rm sail}/\xi h\rho}$$
$$\sim 31.6\sqrt{m_{\rm sail}({\rm kg})/\xi\, h(\mu)\, \rho({\rm g/cc})}$$

$v_0 = \left(\frac{P_0(2\varepsilon_r+(1-\varepsilon_r)\alpha)dD}{c\lambda\alpha_d(\xi D^2 h\rho+m_0)}\right)^{1/2}$ = speed at point where laser spot = sail size.

$P_0 = {v_0}^2 \frac{c\lambda\alpha_d(\xi D^2 h\rho+m_0)}{(2\varepsilon_r+(1-\varepsilon_r)\alpha)dD}$

$L_0 = \frac{dD}{2\lambda\alpha_d}$ = distance at which laser spot = sail size.

Note with $m = m_{\rm sail} + m_0$ we have:

 DOI: 10.5281/zenodo.3747263

$$v_0 = \left(\frac{2P_0(2\varepsilon_r + (1-\varepsilon_r)\alpha)L_0}{mc}\right)^{1/2}$$
$$= \left(\frac{2P_0(2\varepsilon_r + (1-\varepsilon_r)\alpha)L_0}{mc}\right)^{1/2}$$
$$= \left(\frac{2FL_0}{m}\right)^{1/2} = \left(\frac{4P_0L_0}{mc}\right)^{1/2} (\varepsilon_r = 1).$$

With continued illumination the speed increases by $\sqrt{2}$:

$v_\infty = \left(\frac{2P_0(2\varepsilon_r+(1-\varepsilon_r)\alpha)dD}{c\lambda\alpha_d(\xi D^2 h\rho + m_0)}\right)^{1/2}$.

$\mathbf{E_{shot} = P_0 t_0}$ **= main beam energy per shot**

4.1 Non Optimized Case

$$\beta_0 = \left(\frac{P_0(2\varepsilon_r + (1-\varepsilon_r)\alpha)dD}{c^3\lambda\alpha_d(\xi D^2 h\rho + m_0)}\right)^{1/2}$$
$$\rightarrow \left(\frac{2P_0 dD}{c^3\lambda\alpha_d(\xi D^2 h\rho + m_0)}\right)^{1/2} (\varepsilon_r = 1)$$

$$P_0 = {v_0}^2 \frac{c\lambda\alpha_d(\xi D^2 h\rho + m_0)}{(2\varepsilon_r + (1-\varepsilon_r)\alpha)dD}$$
$$= {\beta_0}^2 \frac{c^3\lambda\alpha_d(\xi D^2 h\rho + m_0)}{(2\varepsilon_r + (1-\varepsilon_r)\alpha)dD}$$
$$\rightarrow {\beta_0}^2 \frac{c^3\lambda\alpha_d(\xi D^2 h\rho + m_0)}{2dD} (\varepsilon_r = 1)$$

$$t_0 = \frac{v_0}{a} = \left(\frac{cdD(\xi D^2 h\rho + m_0)}{P_0(2\varepsilon_r + (1-\varepsilon_r)\alpha)\lambda\alpha_d}\right)^{1/2}$$
$$\rightarrow \left(\frac{cdD(\xi D^2 h\rho + m_0)}{2P_0\lambda\alpha_d}\right)^{1/2} (\varepsilon_r = 1)$$

$$E_{\rm shot} = P_0 t_o$$
$$= P_0\left(\frac{cdD(\xi D^2 h\rho + m_0)}{P_0(2\varepsilon_r + (1-\varepsilon_r)\alpha)\lambda\alpha_d}\right)^{1/2}$$
$$= {P_0}^{1/2}\left(\frac{cdD(\xi D^2 h\rho + m_0)}{(2\varepsilon_r + (1-\varepsilon_r)\alpha)\lambda\alpha_d}\right)^{1/2}$$
$$= \beta_0 \frac{c^2(\xi D^2 h\rho + m_0)}{(2\varepsilon_r + (1-\varepsilon_r)\alpha)}$$
$$= \beta_0 \frac{mc^2}{(2\varepsilon_r + (1-\varepsilon_r)\alpha)}$$

$\rightarrow \mathbf{\beta_0 mc^2/2} =$ **(** $\mathbf{\beta_0/2}$**)×system rest mass energy (**$\mathbf{\varepsilon_r = 1}$**)**

$$m = (\xi D^2 h\rho + m_0) = m_{\rm sail} + m_0$$

Note that $E_{\rm shot} = P_0 t_0 = \beta_0 mc^2/2 = \frac{1}{\beta_0} mv^2/2 = \frac{1}{\beta_0}\mathrm{KE}_{\rm system}\,(\varepsilon_r = 1)$.

The product $P_0 t_0$ is ONLY dependent on system mass (m) and the speed.

$\rightarrow \mathbf{P_0 \propto 1/t_0}$ and $\mathbf{t_0 \propto 1/P_0}$ (for fixed speed and mass)

$E_{\rm shot} = P_0 t_0 = \beta_0 mc^2/2 = mvc/2 = p_{\rm system} c/2\,(\varepsilon_r = 1)$ where $p_{\rm system} = mv$ = system momentum.

$\rightarrow\ p_{\rm system} = 2E_{\rm shot}/c = 2p_{\gamma-0} =$ 2×main beam photon momentum (as expected).

The interpretation is that the "shot energy efficiency" $\varepsilon_{\rm shot} \equiv \mathbf{KE_{system}/P_0 t_0} = \mathbf{\beta_0}\ \varepsilon_{\mathbf{shot}} =$ **fraction of main beam photon energy converted to system kinetic energy** where the system mass = $m = m_{\rm sail} + m_0$.

4.2 Optimized Case

$$\beta_0 = \left(\frac{P_0(2\varepsilon_r + (1-\varepsilon_r)\alpha)d}{2c^3\lambda\alpha_d}\right)^{1/2} (\xi h\rho m_0)^{-1/4}$$
$$\rightarrow \left(\frac{P_0 d}{c^3\lambda\alpha_d}\right)^{1/2} (\xi h\rho m_0)^{-1/4} (\varepsilon_r = 1)$$

$$P_0 = {v_0}^2 \left(\frac{(2\varepsilon_r + (1-\varepsilon_r)\alpha)d}{2c\lambda\alpha_d}\right)^{-1} (\xi h\rho m_0)^{1/2}$$
$$\rightarrow {v_0}^2 \left(\frac{d}{c\lambda\alpha_d}\right)^{-1} (\xi h\rho m_0)^{1/2} (\varepsilon_r = 1)$$

$$t_0 = \left(\frac{2cd}{P_0(2\varepsilon_r + (1-\varepsilon_r)\alpha)\lambda\alpha_d}\right)^{1/2} \left(\frac{{m_0}^3}{\xi h\rho}\right)^{1/4}$$
$$\rightarrow \left(\frac{cd}{P_0\lambda\alpha_d}\right)^{1/2} \left(\frac{{m_0}^3}{\xi h\rho}\right)^{1/4} (\varepsilon_r = 1)$$

DOI: 10.5281/zenodo.3747263

$E_{\rm shot} = P_0 t_0 = \beta_0 \frac{mc^2}{(2\varepsilon_r + (1-\varepsilon_r)\alpha)}$ (The product of $P_0 t_0$ is independent of optimization but when optimized $m = 2m_0$)

$\rightarrow \beta_0 m_0 c^2 (\varepsilon_r = 1)$

$\rightarrow$ $E_{\rm shot}/m_0c^2 = \beta_0$ $\rightarrow$ fraction of main beam photon energy compared to bare spacecraft relativistic energy (m_0c^2)=β_0

$\rightarrow$ A large fraction of the photon energy (compared to the base spacecraft relativistic energy) is converted into motion as the spacecraft speed increases.

Note that $E_{\rm shot}/m_0c^2 = \beta_0 \rightarrow E_{\rm shot} = \beta_0 m_0 c^2 = \frac{2}{\beta_0}\frac{m_0 v^2}{2} = \frac{2}{\beta_0}{\rm KE}_{\rm bare-spacecraft}$

$$\begin{aligned}\varepsilon_{\rm shot-bare-spacecraft} &\equiv {\rm KE}_{\rm bare-spacecraft}/P_0 t_0 \\ &= \beta_0/2\end{aligned}$$

$\varepsilon_{\rm shot-bare-spacecraft}$ = fraction of main beam photon energy converted to bare spacecraft kinetic energy

$$\begin{aligned}\varepsilon_{\rm shot} &\equiv {\rm KE}_{\rm system}/P_0 t_0 = \beta_0 \\ &= 2\varepsilon_{\rm shot-bare-spacecraft}.\end{aligned}$$

The time to where the laser spot equals the sail size is (time to L_0):
$t_0 = \frac{v_0}{a} = \left(\frac{cdD(\xi D^2 h\rho + m_0)}{P_0(1+\varepsilon_r)\lambda\alpha_d}\right)^{1/2}$
and $L_0 = \frac{dD}{2\lambda\alpha_d} = \frac{d}{2\lambda\alpha_d}\left(\frac{m_{\rm sail}}{\xi h\rho}\right)^{1/2}$.

The time to where the laser spot equals the sail size for the optimized case where sail mass = payload mass is:

$$\begin{aligned}t_0 &= \left(\frac{2cdD^3\xi h\rho}{P_0(1+\varepsilon_r)\lambda\alpha_d}\right)^{1/2} \\ &= \left(\frac{2cd}{P_0(1+\varepsilon_r)\lambda\alpha_d}\right)^{1/2}\left(\frac{{m_0}^3}{\xi h\rho}\right)^{1/4} \\ &= m_0c^2\left(\frac{2}{P_0(1+\varepsilon_r)P_1}\right)^{1/2}\left(\frac{d}{\alpha_d\xi D}\right)^{1/2} \\ &\sim \frac{m_0c^2}{\sqrt{P_0P_1}}\left(\frac{d}{\alpha_d\xi D}\right)^{1/2} \\ &\sim 1.73\times10^4({\rm s})m_0({\rm kg}) \\ &\quad\times\left(\frac{d}{\alpha_d\xi D}\right)^{1/2}P_0({\rm GW})^{-1/2} \\ &\sim 3.08\times10^3({\rm s})m_0({\rm kg}) \\ &\quad\times\left(\frac{d\sqrt{\xi h(\mu)\,\rho({\rm g/cc})}}{\lambda(\mu)\alpha_d\sqrt{m_0({\rm kg})}}\right)^{1/2}P_0({\rm GW})^{-1/2}\end{aligned}$$

4.3 Laser Aperture Flux

We can calculate the aperture flux as $F_{\rm ap}({\rm W/m^2}) = P_0/\varepsilon_{\rm beam}\xi_{\rm array}d^2$ where $\xi_{\rm array} = 1$ (square laser array) and $\xi_{\rm array} = \pi/4$ (circular array). To achieve a desired speed with a given (fixed) spacecraft mass and sail parameters, the product of P_0 and d must be constant.

Hence to get to a desired $v_0 = \left(\frac{2P_0(2\varepsilon_r+(1-\varepsilon_r)\alpha)dD}{c\lambda\alpha_d(\xi D^2h\rho+m_0)}\right)^{1/2}$ for a fixed sail and spacecraft design with parameters $D, \xi, h, \rho, \varepsilon_r, m_0$ we can vary the system parameters P_0, d, λ but the quantity $P_0 d/\lambda$ must be fixed assuming the array geometry (α_d) is fixed. This means that $P_0 \propto \lambda/d$.

In the optimized case where $m_{\rm sail} = m_0$

$$\begin{aligned}v_0 &= \left(\frac{P_0(2\varepsilon_r+(1-\varepsilon_r)\alpha)d}{2c\lambda\alpha_d}\right)^{1/2}(\xi h\rho m_0)^{-1/4} \\ &\rightarrow P_0 = {v_0}^2\frac{2c\lambda\alpha_d}{(2\varepsilon_r+(1-\varepsilon_r)\alpha)d}(\xi h\rho m_0)^{1/2} \\ &= {\beta_0}^2\frac{2c^3\lambda\alpha_d}{(2\varepsilon_r+(1-\varepsilon_r)\alpha)d}(\xi h\rho m_0)^{1/2}\end{aligned}$$

 DOI: 10.5281/zenodo.3747263

$$F_{\rm ap}({\rm W/m^2}) = P_0/\varepsilon_{\rm beam}\xi_{\rm array}d^2 = \frac{2{\beta_0}^2c^3\lambda\alpha_d}{(2\varepsilon_r+(1-\varepsilon_r)\alpha)\varepsilon_{\rm beam}\xi_{\rm array}d^3} \times (\xi h\rho m_0)^{1/2}.$$

This means the array aperture flux $\mathbf{F}_{\rm ap}({\rm W/m^2}) = \mathbf{P_0}/\varepsilon_{\rm beam}\xi_{\rm array}\mathbf{d^2} \propto \lambda/\mathbf{d^3}$.

This has implications for the system costs. **For example if we make the array 10 times larger the power can be 10 times smaller and the aperture flux will be 1000 times smaller for the same spacecraft speed.**

4.4 Implications for Acceleration Time and Energy Needed

To achieve a desired speed and time to L_0, we can compute the implications of changing the array size and power.

$$t_0 = \left(\frac{cdD(\xi D^2h\rho+m_0)}{P_0(2\varepsilon_r+(1-\varepsilon_r)\alpha))\lambda\alpha_d}\right)^{1/2} \propto \left(\frac{d}{P_0\lambda}\right)^{1/2}$$

but $P_0 \propto \lambda/d$ if we want to achieve the same speed. This means that $t_0 \propto \left(\frac{d}{P_0\lambda}\right)^{1/2} \propto d/\lambda$

To get to a given speed, the time to get to that speed is proportional to the array size. Hence using an array that is 10 times larger (which requires 10 times less power) will require 10 times the time. Note that the energy used is proportional to $P_0t_0 \propto \lambda/d * d/\lambda = 1$. Thus the energy required for a launch to a given speed for given spacecraft and sail parameter does NOT depend on the array size and power modification (keeping P_0d constant, i.e. fixing the speed). This means the energy storage needed per launch is constant with array and power mods.

4.5 Spacecraft and Sail Kinetic Energy

The kinetic energy of the sail and spacecraft to L_0 is calculated in the nonrelativistic limit as the force (which is constant) on the sail times the distance. This neglects the Doppler shift of the impinging photons on the sail which decreases the overall force over the distance L_0.

Kinetic energy to time t_0 is

$${\rm KE} = mv_0^2/2 = \left(\frac{P_0(2\varepsilon_r+(1-\varepsilon_r)\alpha))dD}{2c\lambda\alpha_d}\right) = FL_0.$$

Note this is independent of optimization and overall mass but does depend on sail size D.

While counterintuitive in the context of solar sails, the highest speed is achieved with the smallest sail and thus smallest payload mass (Figure 7). The laser has very narrow bandwidth so we can design the reflector with multilayer dielectric coatings to have ε_r very close to unity.

4.6 Relativistic Corrections

There are several relativistic corrections that modify the nonrelativistic calculations and become important as we proceed to relativistic speeds. The full solution is given in [5], but the physical differences help us understand the corrections:

a) From the viewpoint of the laser the spacecraft reflection/absorption of the photons is redshifted and hence the force is weakened by the reduction of photon energy and momentum. The energy and momentum are conserved by consideration of the photons emitted and returned (if reflected) as redshifted photons. Additionally the moving spacecraft has a perceived increased mass.

If v_0 is the frequency of the photons emitted by the laser and v is the frequency received by the receding spacecraft moving at speed β, then

$$v = v_0\gamma(1-\beta) = v_0\left(\frac{1-\beta}{1+\beta}\right)^{1/2}.$$

For nonrelativistic speeds where β is small, the corrections are of order β: $v = v_0\gamma(1-\beta) \sim v_0(1-\beta)$. The increased relativistic mass of the spacecraft system is $m = m_0\gamma$ where m is the spacecraft system rest mass and and these corrections are modified by γ. Of the two effects the redshift is the most important at lower speeds.

DOI: 10.5281/zenodo.3747263

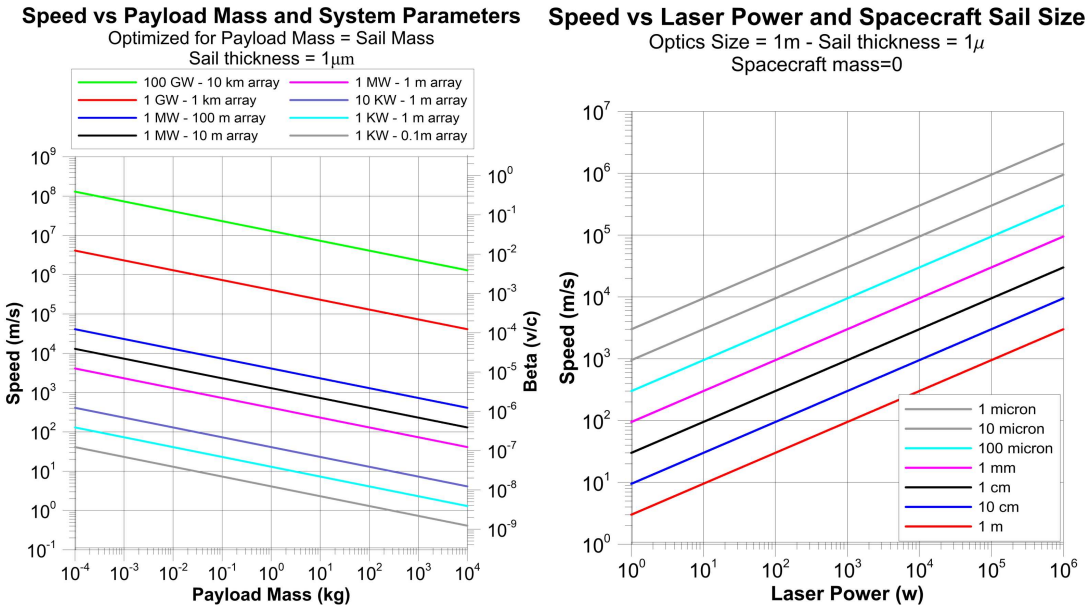

FIGURE 7. ***Left:*** *Speed and Beta vs payload mass vs laser array power and size for systems from very small to very large. This range of systems represents a portion of the roadmap.* ***Right:*** *Speed vs laser power for small systems with 1 m optical aperture vs sail size. All calculations are for the nonrelativistic case.*

b) From the viewpoint of the spacecraft the photons "hitting it" are redshifted as the laser is "perceived" to be receding away. In addition, the rate at which the photons "hit" the spacecraft is reduced due to time dilation. Here the two effects are the same, with the photon redshift being as above, and the time dilation being modified by γ.

These two points of view give the same physical solution but are instructive to understanding the physics of the problem. For high precision calculations, or as we approach the speed of light, the fully relativistic solution detailed in [5] must be used.

4.7 Relativistic Solution

The solution for the case of the beam fully illuminating the sail during time t is shown below. It is given as t versus β (v/c) and $\gamma = (1-\beta^2)^{-1/2}$, assuming $\varepsilon_r = 1$ with $m = m_{\text{sail}} + m_0$ where m_0 = bare spacecraft mass. This assumes the reflector is large enough so that $L < L_0$:

$$t = \frac{mc^2}{6P_0}\left[\frac{(1+\beta)(2-\beta)\gamma}{(1-\beta)} - 2\right]$$

Define $t_E \equiv mc^2/P_0$ ($\equiv$ time for emitted photon energy = spacecraft rest mass energy)

$$\rightarrow t = \frac{t_E}{6}\left[\frac{(1+\beta)(2-\beta)\gamma}{(1-\beta)} - 2\right]$$

In the nonrelativistic limit this becomes:

$$t_{\text{NR}} = \frac{t_E}{2}\beta = \frac{mcv}{2P_0}(\beta << 1)$$

$$t/t_{\text{NR}} = \frac{1}{3\beta}\left[\frac{(1+\beta)(2-\beta)\gamma}{(1-\beta)} - 2\right]$$

The time to a given speed and distance is longer and the speed at a given distance is lower in the relativistic solution. For low β the difference is small (see Figure 8).

Using conservation of momentum for the entire photon and spacecraft system, we obtain the equations of motion for the relativistic case as:

$$\dot{\beta} = \begin{cases} \frac{2P_0}{mc^2\gamma^3}\left(\frac{1-\beta}{1+\beta}\right) & x < L_0 \\ \frac{2P_0}{mc^2\gamma^3}\left(\frac{1-\beta}{1+\beta}\right)\left(\frac{L_0}{x}\right)^2 & x > L_0 \end{cases}$$

We can integrate this directly noting that $d\beta/dt = d\beta/dx * dx/dt = c\beta * d\beta/dx$. We

 DOI: 10.5281/zenodo.3747263

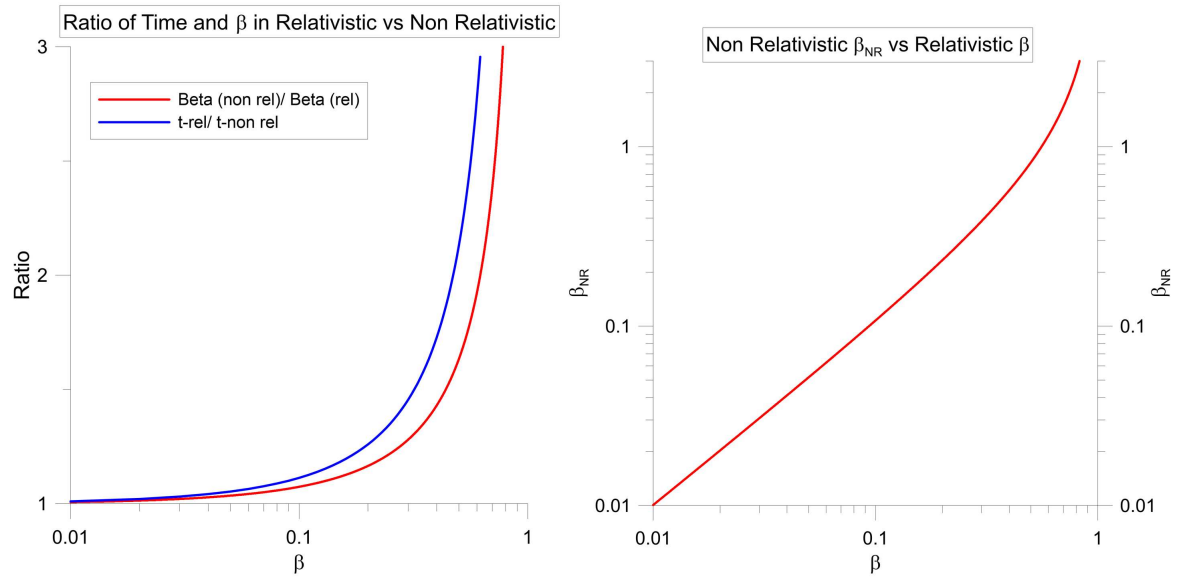

FIGURE 8. ***Left:*** *Semilog plot of $\beta/\beta_{\rm NR}$ and $t/t_{\rm NR}$ as a function of β.* ***Right:*** *Log-log plot of nonrelativistic β as a function of β.*

then get:

Noting $\int \beta(1-\beta)^{-5/2}(1+\beta)^{-1/2}d\beta = \frac{2\beta-1}{3\gamma(1-\beta)^2} + \text{const}$

$$\frac{2\beta-1}{3\gamma(1-\beta)^2} + \frac{1}{3} = \frac{2P_0}{mc^3}x \quad \text{for } x < L_0$$

The speed β_0 at L_0 is thus given by:

$$\rightarrow \frac{2\beta_0-1}{3\gamma_0(1-\beta_0)^2} + \frac{1}{3} = \frac{2P_0}{mc^3}L_0 = \frac{2P_0}{mc^2}\frac{L_0}{c} = 2\frac{t_L}{t_E}$$

where $t_L \equiv L_0/c =$ light travel time over distance L_0.

Expanding this to order ${\beta_0}^2$ we have (at small β_0):

$$\begin{aligned}\frac{2\beta_0-1}{3\gamma_0(1-\beta_0)^2} + \frac{1}{3} &= \frac{2\beta_0-1+\gamma_0(1-\beta_0)^2}{3\gamma_0(1-\beta_0)^2} \\ &\sim \frac{2\beta_0-1+(1+\frac{{\beta_0}^2}{2})(1-\beta_0)^2}{3\gamma_0(1-\beta_0)^2} \\ &= \frac{{\beta_0}^2(\frac{3}{2}-\beta_0)}{3\gamma_0(1-\beta_0)^2} \sim \frac{{\beta_0}^2}{2}\end{aligned}$$

$\rightarrow {\beta_0}^2 = 4\frac{t_L}{t_E}$ (for small β_0, or nonrelativistic limit)

This is identical to the nonrelativistic limit derived earlier of:

$$\beta_{0-\rm NR} = \sqrt{\frac{4P_0}{mc^3}L_0} = \sqrt{4\frac{t_L}{t_E}}$$

We can rewite the relationship between the correct relativistic speed β_0 at L_0 compared to the nonrelativistic speed $\beta_{0-\rm NR}$ solution as below. The same relationship holds at any point up to L_0. Note that the nonrelativistic $\beta_{0-\rm NR}$ always overestimates the correct speed β_0 up to and including at L_0.

$$\frac{2\beta_0-1}{3\gamma_0(1-\beta_0)^2} + \frac{1}{3} = \frac{2P_0}{mc^3}L_0 = 2\frac{t_L}{t_E} = \frac{{\beta_{0-NR}}^2}{2}$$

$$\rightarrow \beta_{0-NR} = \sqrt{2}\left[\frac{2\beta_0-1}{3\gamma_0(1-\beta_0)^2} + \frac{1}{3}\right]^{1/2}$$

$$\rightarrow \frac{\beta_{0-NR}}{\beta_0} = \frac{\sqrt{2}}{\beta_0}\left[\frac{2\beta_0-1}{3\gamma_0(1-\beta_0)^2} + \frac{1}{3}\right]^{1/2}$$

The relationship between the nonrelativistic and relativistic solutions is particularly useful in that the computations and insight from the nonrelativistic solutions

DOI: 10.5281/zenodo.3747263

are much easier, and the given ratios of $t/t_{\rm NR}$ and $\beta_0/\beta_{0-\rm NR}$ allow us to compute $\beta_{0-\rm NR}$ and $t_{0-\rm NR}$ from the system parameters and then translate to the relativistic solution for β_0 and t_0. For example, at $\beta_0 = 0.10$ $\beta_{0-\rm NR}$ is computed to be 8% higher than it should be, at $\beta_0 = 0.20$ $\beta_{0-\rm NR}$ is 16% higher than it should be, and at $\beta_0 = 0.30$ $\beta_{0-\rm NR}$ is 28% higher than it should be. The full relativistic solution can and is to be used, but it is less intuitive and often the nonrelativistic solution for mildly relativistic systems gives much more insight into the system design. For highly relativistic solutions it is easier to use the fully relativistic solution.

4.8 Optimization of Reflector and Spacecraft Mass in the Relativistic Limit

In the nonrelativistic limit we showed that the maximum speed is obtained when the reflector mass is equal to the spacecraft mass [4]. In the full relativistic case the same condition holds, namely the maximum speed is when the reflector and spacecraft mass are equal ($m_{\rm sail} = m_0$) [5].

4.9 Energy and Momentum Transfer -- Photon-Electron Interactions

It is important to understand the basic photon-electron interaction. If the photon-electron (reflector) collision is purely elastic and the reflector is at rest in the frame of the photon emitter, then the photon energy is the same after reflection as before and there can hence be no energy transfer from the photon to the sail. The momentum of the photon changes (it is going in the opposite direction after reflection), therefore momentum is exchanged with the reflector, but no energy is exchanged. How can this be? This is a classic and interesting problem in energy transfer. A good analogy is to consider the nonrelativistic energy during momentum exchange, in a completely elastic collision, where the kinetic energy of the object (reflector in this case) undergoes a momentum change from the photons of $2E/c$ where E is the incident photon energy. The kinetic energy of the reflector is then KE = $p^2/2m = 2E^2/mc^2$ where m is the mass of the reflector. The only way to maintain energy conservation here is if KE = 0, which is only possible if $m = \infty$. What actually happens in a finite mass reflector is that the reflector recoils slightly during the photon-electron interaction and the photon reflected does NOT have the same energy as the incident photon. During the photon-electron interaction the electron is coupled to the lattice which then recoils and the reflected photon is slightly Doppler shifted. This effect is ultimately what is responsible for the reflector starting to move. It is also why the photon-electron energy transfer efficiency increases as the speed of the reflector increases (see efficiency section below). A relativistic discussion of this is given in [5].

4.10 Energy Required per Launch

The energy required per launch is helpful in planning a system design, as there may be a need to store the energy rather than have a continuous mode. This would have the effect of lowering the capacity of the electrical power system and allow a "trickle charge mode." We define E_γ as the photon energy in the main beam (on the sail) to get to the point where the spot size equals the reflector size. Thus $E_\gamma = P_0 * t_0$. In general we will increase the illumination time by a factor of a few times greater than t_0 in order to get most of the factor of $\sqrt{2}$ increase in speed that comes from continued illumination in the nonrelativistic case. There is little need for additional continued illumination since the speed increase is of diminishing return beyond a few times t_0.

The electrical energy $E_{\rm elec}$ use over time t_0 is $E_{\rm elec} = E_\gamma/(\varepsilon_{\rm elec} * \varepsilon_{\rm beam}) = P_0 * t_0/(\varepsilon_{\rm elec} * \varepsilon_{\rm beam})$ where $\varepsilon_{\rm elec}$ is the total electrical to overall photon conversion efficiency ($\varepsilon_{\rm elec} = P_{\rm optical}/P_{\rm electrical}$) and includes all efficiencies such as power supply, laser amplifier, etc. $P_{\rm optical}$ is the total photon power emitted by the laser array. As an example, the current "wall plug" efficiency of the Yb laser amplifiers is about 0.42. Note $P_0 = \varepsilon_{\rm beam} P_{\rm optical} = (\varepsilon_{\rm elec} * \varepsilon_{\rm beam}) P_{\rm electrical}$.

Total photon energy in the main beam (on the sail) to time t_0:

$$
\begin{aligned}
E_\gamma = P_0 t_0 &= P_0 \left(\frac{cdD(\xi D^2 h\rho + m_0)}{P_0(1+\varepsilon_r)\lambda\alpha_d} \right)^{1/2} \\
&= \left(\frac{cdD(\xi D^2 h\rho + m_0)P_0}{(1+\varepsilon_r)\lambda\alpha_d} \right)^{1/2} \\
&= m_0 c^2 \left(\frac{2P_0}{(1+\varepsilon_r)P_1} \right)^{1/2} \left(\frac{d}{\alpha_d \xi D} \right)^{1/2} \\
&\sim m_0 c^2 \left(\frac{P_0}{P_1} \right)^{1/2} \left(\frac{d}{\alpha_d \xi D} \right)^{1/2}
\end{aligned}
$$

 DOI: 10.5281/zenodo.3747263

for the optimized case (sail=payload mass + ε_r=1 in last term).

We define the (main beam) launch energy efficiency to time t_0 as:

$$\begin{aligned}\varepsilon_{\rm launch} &\equiv {\rm KE}(t_0)/E_\gamma \\ &= \left(\frac{P_0(1+\varepsilon_r)dD}{2c\lambda\alpha_d}\right) \\ &\quad \times \left(\frac{cdD(\xi D^2 h\rho + m_0)P_0}{(1+\varepsilon_r)\lambda\alpha_d}\right)^{-1/2} \\ &= \frac{(1+\varepsilon_r)}{2c}\left(\frac{P_0(1+\varepsilon_r)dD}{c\lambda\alpha_d(\xi D^2 h\rho + m_0)}\right)^{1/2} \\ &= \frac{(1+\varepsilon_r)}{2c}v_0 = \frac{(1+\varepsilon_r)}{2}\beta_0.\end{aligned}$$

Note the launch efficiency does NOT depend on optimization (sail mass = payload mass) and for $\varepsilon_r = 1$ then $\varepsilon_{\rm launch} = \beta_0$.

The total electrical energy used to time t_0 for a given v_0 is:

$$E_{\rm elec} = E_\gamma/(\varepsilon_{\rm elec}\varepsilon_{\rm beam}).$$

We can see the relatively simple scaling for photon energy used per launch (to time t_0) in terms of the rest mass energy of the spacecraft, the power P_0, the array size d and reflector size D. The reason the photon energy scales with the array size as $d^{1/2}$ is due to the fact that a larger array will have a smaller spot and thus a longer illumination time. The distance L_0 to where the spot size equals the reflector size is $L_0 = dD/2\lambda$ and thus L_0 is proportional to the array size d. Since the acceleration is constant while the beam is contained within the reflector ($L < L_0$) we have $L_0 = at_0^2/2$ and thus $t_0 = (2L_0/a)^{1/2}$, hence t_0 scales as $L_0^{1/2}$ or as $d^{1/2}$.

4.11 Efficiency

The instantaneous energy efficiency (power that goes into direct kinetic energy/laser power on reflector) is:

$$\begin{aligned}\varepsilon_p &= \frac{d{\rm KE}}{dt}/P_0 = mva/P_0 \\ &= mvP_0(1+\varepsilon_r)/mcP_0 = \beta(1+\varepsilon_r) \\ &= ma^2t/P_0 = P_0t(1+\varepsilon_r)^2/mc^2 \\ &\sim 2\beta \sim 4P_0t/mc^2 \text{ for } \varepsilon_r \sim 1\end{aligned}$$

and total integrated energy efficiency ($\varepsilon_p \sim t$) is:

$$\begin{aligned}\varepsilon_{\rm total} &= 1/2\varepsilon_{\rm p} = \beta(1+\varepsilon_r)/2 \\ &= P_0t(1+\varepsilon_r)^2/2mc^2 \sim \beta \\ &\sim 2P_0t/mc^2 \text{ for } \varepsilon_r \sim 1\end{aligned}$$

where $m = m_{\rm sail} + m_0$. See launch efficiency above.

Momentum "efficiency" $= (1+\varepsilon_r) \sim 2$ for $\varepsilon_r \sim 1$ with $\beta << 1$. The energy transfer efficiency starts at very low levels and then increases proportionally with the speed. The total integrated energy efficiency is just half that of the instantaneous efficiency at the final speed since the force is constant as long as the laser spot is smaller than or equal to the reflector size, hence the acceleration is constant and the speed increases proportionally with time ($\beta \propto t$), thus the average ε_p is half the maximum β achieved. This is for the nonrelativistic case. For spacecraft accelerated to high speeds the energy efficiency can become quite high.

4.12 Flux on Sail

The scaling of flux on the reflector is:

$$\begin{aligned}\text{Flux} &= P_0/\text{cross sectional area of sail} \\ &= P_0/\xi D^2\end{aligned}$$

1) Square and Circular sail
Assuming an optimized case where sail mass = payload mass ($m_0 = m_{\rm sail} = \xi_{\rm square,cir}D^2h\rho$)

$D = (m_0/\xi_{\rm square,cir}h\rho)^{1/2}$
Flux $= P_0/\xi_{\rm square,cir}D^2 = P_0h\rho/m_0$
Square: $\xi_{\rm square} = 1$, Circular: $\xi_{\rm cir} = \pi/4$

2) Spherical sail
Assuming an optimized case where sail mass = payload mass ($m_0 = m_{\rm sail} = \xi_{\rm sphere}D^2h\rho$)

$D = (m_0/\xi_{\rm sphere}h\rho)^{1/2}$
Flux $= P_0/\xi_{\rm cir}D^2 = P_0\xi_{\rm sphere}h\rho/\xi_{\rm cir}m_0$
$= 4P_0h\rho/m_0$

$\xi_{\rm cir} = \pi/4$ (circular cross section)
$\xi_{\rm sphere} = \pi$

Note the flux is proportional to the thickness and density (smaller sail) and inversely proportional to

the mass (larger sail). This means lower mass payloads have high flux requirements on the sail (see Figure 9).

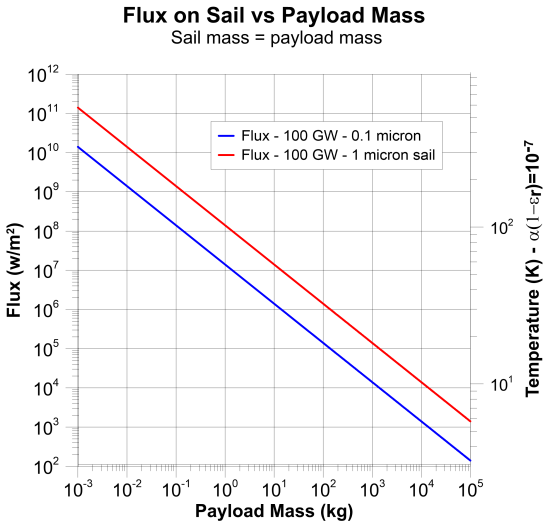

FIGURE 9. *Optical intensity incident on light sail as a function of payload mass, in the optimized case where $m_0 = m_{\rm sail}$ for two sail thicknesses of 0.1 and 1 μm. Sail temperature for $\alpha = 10^{-7}$ is also shown assuming zero background temperature.*

4.13 Reflectors with Both Absorption and Reflection

We consider the case of a reflector that is both reflective and absorptive. This is the general case for all materials, though we will often be in the highly reflective regime. In the general case we compute the force by considering both the reflective and absorptive components. Both the reflection coefficient ε and the absorption coefficient α are dependent on the angle of incidence θ_n (relative to the local surface normal). The force F on a small region illuminated by power P_0 where θ_n does not change much is given by:

$$F = \frac{dp}{dt} = \frac{2P_r}{c} + \frac{P_A}{c} = \frac{P_0}{c}\,(2\varepsilon_r + (1-\varepsilon_r)\alpha)$$

$\alpha =$ absorption coefficient

IF $\alpha = 1$ (complete **absorption inside reflector of the part not reflected**), then:

$$F = \frac{dp}{dt} = \frac{P_0}{c}(2\varepsilon_r + (1-\varepsilon_r)) = \frac{P_0(1+\varepsilon_r)}{c}$$

P_0 = Laser power at reflector

P_r = Laser power reflected at first surface = $P_0\varepsilon_r$

P_A = Laser power absorbed inside reflector = $P_0(1-\varepsilon_r)\alpha$

P_T = Laser power transmitted through reflector = $P_0 - P_r - P_A$

$P_0 = P_r + P_A + P_T$

ε_r = reflector reflection coefficient

ε_r = 1 for perfect reflection

ε_r = 0 for no reflection

α = 0 for no absorption of light inside reflector

α = 1 for complete absorption of light inside reflector (i.e. no transmission)

Note that for metalized reflectors $\alpha \approx 0.01$ since radiation not reflected is absorbed unless the metal is very thin (less than a skin depth). The general case would then replace $\mathbf{P_0(1+\varepsilon_r)}$ by $\mathbf{P_0(2\varepsilon_r + (1-\varepsilon_r)\alpha)}$.

The local radiation pressure at point $\mathbf{X}$ on the reflector with flux is then:
$p_{\rm rad-press}(\mathbf{X}) = F_{\rm flux}(\mathbf{X})(1+\varepsilon_r)/c$ if there is complete absorption ($\alpha = 1$).

Or more generally:
$p_{\rm rad-press}(\mathbf{X}) = F_{\rm flux}(\mathbf{X})(2\varepsilon_r + (1-\varepsilon_r)\alpha)/c$.

4.14 Sail Temperature

We can compute the approximate sail temperature $T_{\rm sail}$ based on the absorption coefficient and the effective emissivity of the front and back of the sail, assuming equal temperature on front and back. In the case of an inflated sail the thermal connection between the front and back surfaces is generally very low and hence the area of the sail below is just the "front facing" area. For simplicity we assume the background temperature (flux) is zero.

 DOI: 10.5281/zenodo.3747263

ε_f = emissivity (convolved) of front of sail

ε_b = emissivity (convolved) of back of sail

$A_{\rm sail}$ = sail area

$$F_{\rm flux} = P_A/A_{\rm sail} = \alpha P_0(1-\varepsilon_r)/A_{\rm sail} \\ = \sigma T^4(\varepsilon_f + \varepsilon_b)$$

where P_0 is the power in the main beam on the sail

$$T_{\rm sail} = [\alpha P_0(1-\varepsilon_r)/\sigma(\varepsilon_f+\varepsilon_b)A_{\rm sail}]^{1/4}$$

See Figure 10 for plots of $T_{\rm sail}$ as a function of α and ε_r for different values of P_0. The maximum admissible sail temperature will depend on the material. Plastics can survive temperatures up to 400-500 Kelvin, while glasses can withstand 1000 Kelvin and above.

4.15 Levitation and Low Acceleration Tests

In preliminary testing, the ability to levitate a sail and study its stability when perturbed will be important. Assuming a vertical test with the laser below and sail we can calculate the sail flux as follows:

$F_T = P_0(1+\varepsilon_r)/c - mg$
$a = F_T/m = P_0(1+\varepsilon_r)/mc - g$
$P_0 = mc(a+g)/(1+\varepsilon_r)$
where the total system mass is $m = m_{\rm sail} + m_0 = (\xi D^2 h\rho + m_0)$
$\xi D^2 = (m-m_0)/h\rho$

1) Square and Circular sail

$$\text{Flux} = P_0/\xi_{\rm square,cir}D^2 = P_0 h\rho/(m-m_0) \\ = \frac{h\rho mc(a+g)}{(1+\varepsilon_r)(m-m_0)} \\ \rightarrow \frac{h\rho c(a+g)}{(1+\varepsilon_r)} \ (m_0=0)$$

Square: $\xi_{\rm square} = 1$
Circular: $\xi_{\rm cir} = \pi/4$

2) Spherical sail
Assuming an optimized case where sail mass = payload mass $m_0 = m_{\rm sail} = \xi_{\rm sphere}D^2 h\rho$:

$\xi_{\rm sphere}D^2 = (m-m_0)/h\rho$

$$\text{Flux} = P_0/\xi_{\rm cir}D^2 \\ = P_0\xi_{\rm sphere}h\rho/\xi_{\rm cir}(m-m_0) \\ = \frac{4h\rho mc(a+g)}{(1+\varepsilon_r)(m-m_0)} \\ = \frac{4h\rho c(a+g)}{(1+\varepsilon_r)} \ (m_0=0)$$

$\xi_{\rm cir} = \pi/4$ (circular cross section)
$\xi_{\rm sphere} = \pi$

Note that the sail flux only depends on the sail thickness and density for $m_0 = 0$ (no payload) assuming $\varepsilon_r = 1$. See Figure 11 for a plot of levitation flux as a function of sail thickness. The power per unit mass is 1.5 kW/mg.

5 Scaling

Since the **system we propose is not single use but rather scalable to any size, it is critical to understand the scaling relations in the section above.** In general we use the optimized case of payload mass = sail mass and assume a nearly ideal sail tuned to the laser wavelength so $\varepsilon_r = 1$. We assume a slightly futuristic sail with thickness of 1 μm for many cases and 10 μm (thick even for today's sails). Future advancements in sail thicknesses down to 0.1 μm and below can be envisioned but are NOT assumed. They will only make the conclusions even more optimistic. The density of all sails we consider is about the same, namely $\rho \sim 1,400\ {\rm kg/m^3}$ (1.4 times that of water). We can then vary power, laser array size and payload mass as we proceed along the roadmap from small to large systems. The trade-offs between payload mass, speed desired, power and array size required are then explored. We cover this much more in our papers, but the basic conclusions are as stated, namely payloads from wafer scale and below to 10^5 kg and above (human capable) can all be propelled, albeit with different speeds. For $\varepsilon_r = 1$ we have (optimized case):

$$v_{\rm max-\infty} = \left(\frac{2P_0 d}{c\lambda a_d}\right)^{1/2}(\xi h\rho m_0)^{-1/4}$$

which scales as $P_0^{1/2}$, $d^{1/2}$, $\lambda^{-1/2}$, $h^{-1/4}$, $\rho^{-1/4}$, and $m_0^{-1/4}$. The scaling of speed is a mild function of pay-

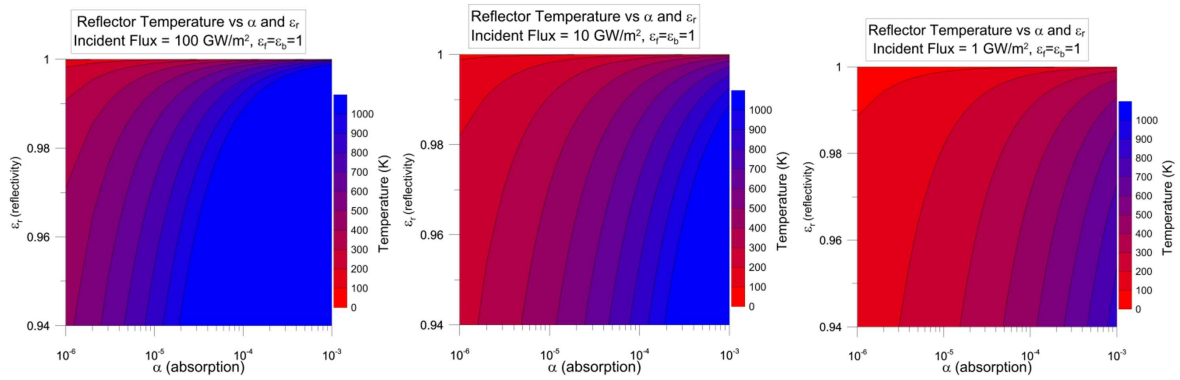

FIGURE 10. *Sail temperature as a function of absorption and reflection coefficients for different values of laser power.*

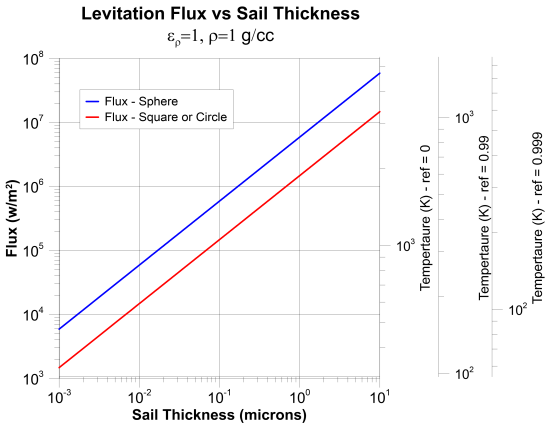

FIGURE 11. *Optical intensity required to levitate a sail as a function of sail thickness, assuming perfect reflectivity and mass density of 1 g/cc. The power per unit mass is 1.5 kW/mg.*

load mass ($\propto m_0^{-1/4}$). This relationship is due to the fact that the sail size increases with payload mass. As the sail size grows, the acceleration distance increases as the laser spot can become larger. These effects mitigate the detriment of increased mass. So while a gram scale wafer can be accelerated to relativistic speeds ($c/4$ in our largest baseline case – DE-STAR 4), the same laser array that accomplishes this can also propel a 100 kg craft (Voyager class) to about 1.5% c, or nearly 300 times faster than what Voyager achieved after 37 years. A 100 kg craft of this type would reach 1 AU ($\sim$ Mars) in about a day while a Shuttle class vehicle with a mass of 10^5 kg ($\sim$ 100 tons) would reach 0.26% c, or about 780 km/s, 46 times faster than Voyager. This exceeds the galactic escape speed for example (depending on the Dark Matter distribution). While the numbers may be mind-numbing, they need to be kept in context. **This system is NOT only for small spacecraft.** We are also NOT proposing we should immediately build the largest system, but rather begin the roadmap to do so.

For high mass nonrelativistic missions in our solar system, another approach that uses the same core laser array technology is to beam power to the spacecraft but use photoconversion (PV) on the spacecraft to generate electrical power to drive a high I_{sp} ion engine.

6 Eye Safety Limits in Ground Testing

We plot the accepted maximum permissible exposure (MPE) limits for lasers in the visible and near IR including the nominal baseline Yb 1.064 μm band versus exposure time in Figure 12. For exposures beyond 10 seconds we are in the continuous wave (CW) limit (essentially unlimited exposure), which is the most restrictive. We adopt the CW limit as the value we seek to stay below for all exposures. Note that at 1.064 μm the CW limit is 5 mW/cm^2 or 50 W/m^2.

6.1 Ground Testing -- Rayleigh and Particulate Backscatter

For ground testing the issues of molecular (Rayleigh) scattering, as well as scattering from particulates such as dust and ice crystals in the atmosphere, need to be considered to determine any possible hazards, particu-

 DOI: 10.5281/zenodo.3747263

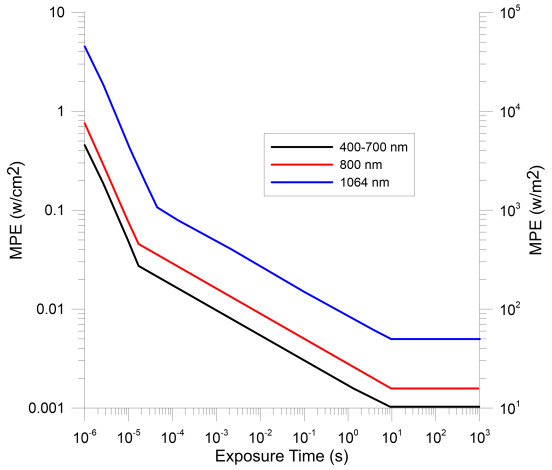

FIGURE 12. *Maximum permissible exposure (MPE) as a function of exposure time. For 1.064 μm radiation in the continuous wave limit (exposure time $\rightarrow \infty$), the MPE is 5 mW/cm^2.*

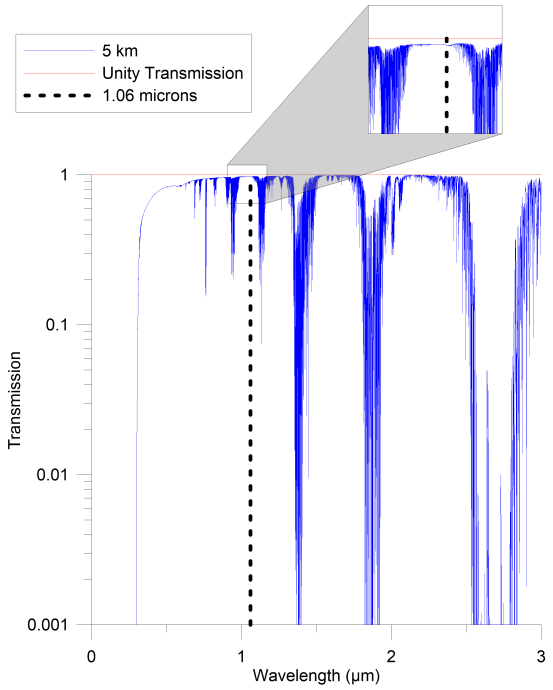

FIGURE 13. *Atmospheric transmission as a function of wavelength. The transmission at our proposed wavelength of 1.06 microns is close to unity.*

larly to human and animal eyes. We can make a first-order estimate by assuming all of the transmission loss ε from ground to space is due to scattering rather than absorption. This is an upper limit. As shown in Figure 13, for a clear day at a 5 km site the transmission loss is less than $\varepsilon = 0.03$. We will assume that the scattered light is all emitted in one scale height for N_2, O_2 which is about $\delta = 8$ km for a standard atmosphere. Assuming a cylindrical distribution of the scattered light we can calculate the scattered light flux $F_{\rm scatt}$ versus distance R from the center of the array (see Figure 14) for a given array emitting optical power P as $F_{\rm scatt}(R) = \varepsilon P/2\pi R\delta$. For $R = 1000$ m (500 m from edge of 1 km array), $\varepsilon = 0.03$, $\delta = 8000$ m, $P = 100$ GW we get $F_{\rm scatt}$ ($R = 1$ km) = 60 W/m^2, or just very slightly above the MPE at 1.06 μm. This is encouraging.

The atmosphere is a complex mixture of N_2, O_2, H_2O, dust, aerosols etc. that is spatially and temporally varying, and these need to be measured and factored in before high level power is emitted for each "shot." Monitoring of the scattered light is easy to do by placing narrowband filtered photodetectors (photodiodes or Si CMOS imagers which just barely work at 1.06 μm) to monitor each "shot." Monitoring ground animals near the array as well as birds that may fly near the array will be necessary to avoid eye damage.

7 Reflector Back Illumination Hazards

The issue of reflection off the main sail back towards the Earth is critical to understand in terms of safety for ground testing, ground deployment, and space based deployment. There are several simple approaches to this. One is to roughen the reflective surface slightly ("small scale glint") and the other is to prevent any significant "flat areas" to prevent "large scale glint." We can estimate the scale size of the "specular reflection regions or glint region size" allowed. If we assume a flat surface region of the reflector size $D_{\rm flat}$ for a reflector of total size D illuminated with main beam power P_0 at a distance L from the Earth, we can compute the "back scatter flux" $F_{\rm back}$ at the Earth assuming the specular reflection region results in a diffraction limited return spot:

$$F_{\rm back} = P_0(D_{\rm flat}/D)^2/(L * 2\lambda/D_{\rm flat})^2$$
$$= P_0 D_{\rm flat}^4/(4L^2\lambda^2 D^2).$$

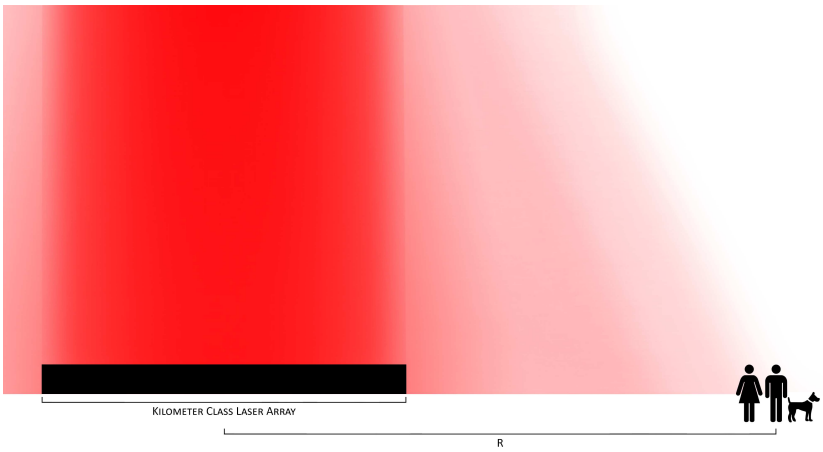

FIGURE 14. *Backscatter illumination at a distance R from the center of a laser array.*

Solving for the maximum allowed specular region size $D_{\rm flat}$ for a given maximum allowed $F_{\rm back}$ (which is typically set by the MPE for eye exposure), we get:

$$D_{\rm flat} = [4L^2\lambda^2 D^2 F_{\rm back}/P_0]^{1/4}.$$

See Figure 15 for a plot of $D_{\rm flat}$ as a function of L for different values of P_0 and for $F_{\rm back} = 5$ mW/cm^2 (MPE at 1.06 μm). Since the sail shape will subject to extremely large accelerations during the launch phase for small mass payloads, it is important to consider this issue carefully to minimize glint concerns.

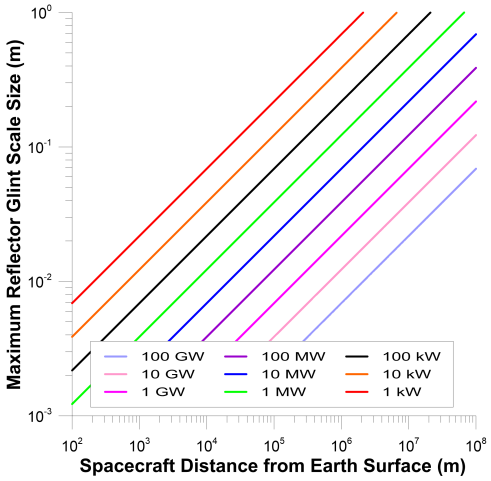

FIGURE 15. *Maximum flat surface size of a sail reflector as a function of distance from Earth for different laser power values. Assumes $F_{\rm back} = 5$ mW/cm^2 (MPE at 1.06 μm).*

8 Beam Sidelobes and Hazards to Aircraft and Satellites

With the anticipation of extremely large power levels, the issue of beam spillover and particularly that of sidelobes accidentally hitting an aircraft, bird or orbital asset must be considered. For example, even a 30 db sidelobe would amount to a 100 MW beam if the main beam were 100 GW. This sidelobe "illumination" is an extremely large amount of power and needs to be carefully managed. Due to various noise sources, the sidelobes will also move spatially and temporally. Detailed modeling and measurements of the sidelobe structure and knowledge of all targets in the extended field of view that may be impacted will need to be a part of an operational system. In addition, the beam pattern will change due to the rapid F# change and Fresnel (near field) beam effect variations in the optical pattern as the spacecraft moves away. However, the beam size is close to the aperture size for airborne and LEO assets and hence the flux is relatively low because the beam is focused on the spacecraft at much greater distances.

9 Array Ground Testing and Deployment Option

The trade-off between space deployment and ground deployment of the photon driver is not a simple one. The early testing will be ground based for both economic and rapid technical feedback reasons. In the

 DOI: 10.5281/zenodo.3747263

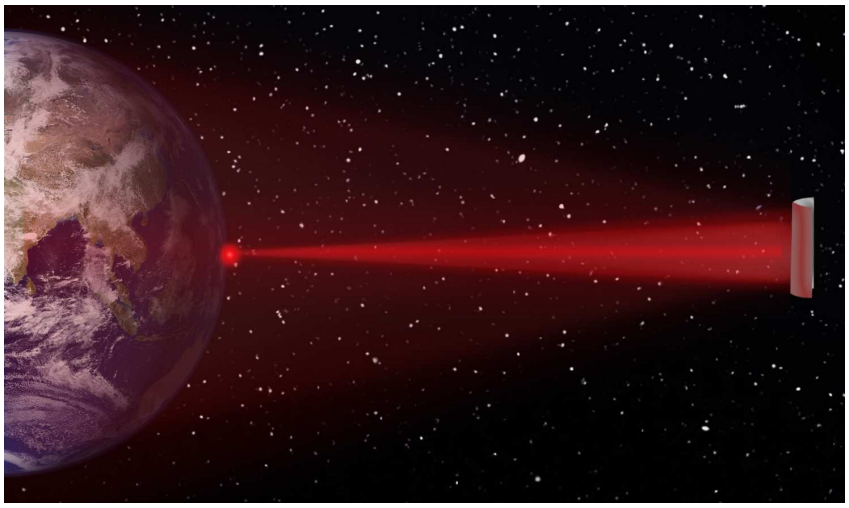

FIGURE 16. *Reflector accelerated by an Earth-based laser.*

longer term, a fundamental question yet to answered is, "Can we achieve near diffraction limited performance (high Strehl ratio) for a large aperture ground based system?" We will not know the answer to this until we perform the relevant system level tests with sparse laser arrays at large baselines. Even if we can adequately mitigate the atmospheric issue, there is still a fundamental set of limits that ground deployment has. These limits include issues with sidelobe spillover onto other space assets as well as airplanes and birds, for example. One of the more serious problems with ground deployment is the severe targeting limitation it imposes in terms of the location of the ground photon driver and the desired target. These issues are discussed further in section 20. In spite of all these limitations, the economic issue outweighs the technical and programmatic issues, so that initial testing and deployment will be ground based with the primary issue then being one of atmospheric mitigation, which is detailed in subsections 9.1 and 9.2.

The Earth's atmosphere is a complex mixture of molecules, with Oxygen and Nitrogen being well mixed and water vapor not being well mixed. Oxygen and Nitrogen have a scale (e-folding) height of about 8 km while water has a scale height of about 2 km. Typical good ground based sites are either mountains or high plateaus at mid-latitudes or in the Antarctic. All of these locations have challenges in construction and deployment. Early testing (low power) will likely be done at existing astronomical or related facilities at altitudes of 4-5 km. Our White Mountain research station is one of the sites we will use. If a target such as Alpha Centauri is chosen, then the Southern Hemisphere must be used since the declination of Alpha Centauri is about $\delta = -61$ deg and Proxima Centauri about $\delta = -63$ deg. Suitable sites would be in Chile or Antarctica. However, another complication is that of the spacecraft deployer as the launch site; the deployer and target must be nearly inline. An advantage of the Antarctic plateau, in addition to the excellent transmission and seeing, is that being at or near a geographic pole makes targeting and tracking simpler. Examples of good sites in Antarctica are the South Pole and Domes A, C and F and related areas. The deployment and construction, power, etc. would be formidable however. For a global analysis of the atmospheric conditions of all ground sites see [6].

For some elements of the test program, high altitude testing is extremely useful. The air density roughly decreases exponentially with altitude for the uniformly distributed components (O_2 and N_2), as well as with water vapor. Much of the absorption in the bands of interest is strongly influenced by water vapor content. The "seeing" is also highly dependent on altitude as well as "local weather" variations. Day and nighttime transparency is nearly the same for all other factors being equal while the "seeing" metric C_n^2 is often highly sensitive to day-night transitions. These metrics are critical to understand for ground based testing and deployment as well as airborne testing.

DOI: 10.5281/zenodo.3747263

9.1 Ground Based Atmospheric Perturbations -- Seeing Issues

The Earth's atmosphere introduces many challenges for ground based operations. One of the most difficult is the "seeing" issue due to perturbations in the temperature and pressure of the atmosphere along the line of sight. While well studied, the turbulent flow in the atmosphere is still not understood at the level that we desire. We show modeled atmospheric index of refraction versus altitude based on temperature and pressure balloon borne measurements. This is often characterized by the correlation parameter C_n^2. If we assume a Kolmogorov theory and spectrum for the atmospheric fluctuations we can relate the C_n^2 values to the effective angular perturbations $\theta_{\rm FWHM}$ to what is often known as the "Fried coherence length" r_0 as shown below. Typical values for C_n^2 at the Earth's surface are 10^{-12} (poor seeing) to 10^{-16} (very good seeing) while at high altitudes (30+ km) C_n^2 can be less than 10^{-19}.

$$C_n{}^2(x) = \left\langle [n(x) - n(x+r)]^2 \, r^{-2/3} \right\rangle$$

$$= D_n r^{-2/3}$$

where n is the index of refraction, x is a spatial position in the atmosphere, r is the separation distance within the eddy scale between the inner scale (dissipation) and outer scale (production) and D_n is the index of refraction structure function. Note that the units of $C_n{}^2$ are $\mathrm{m}^{-2/3}$.

$$r_0(\lambda, h) \quad = \quad \left[0.423 \left(\tfrac{2\pi}{\lambda}\right)^2 \sec\delta \int_h^\infty C_n{}^2(x) dx \right]^{-3/5}$$

= Fried parameter $\sim$ eq. isoplanatic patch size, δ = obs zenith angle.

$\Theta_{\rm FWHM}(\lambda, h) = 0.98\lambda / r_0(\lambda, h)$ = seeing disk size $\sim$ diffraction limited resolution for optic of size $r_0(\lambda, h)$.

Note that $r_0(\lambda, h) \sim \lambda^{6/5}$ and that $\Theta_{\rm FWHM}(\lambda, h) = 0.98\lambda / r_0(\lambda, h) \sim \lambda^{-1/5}$ (thus varies slowly with λ).

It can be shown that the phase variance ($\sigma_\phi{}^2$) over an aperture of diameter r_0 is $\sigma_\phi{}^2(D = r_0) = 1.03\,\mathrm{rad}^2$. Similarly it can be shown the phase variance over an aperture of diameter D is $\sigma_\phi{}^2(D) = 1.03(D/r_0)^{5/3}\,\mathrm{rad}^2$.

The exponent of 5/3 comes from the assumed Kolmogorov spectrum of turbulent dissipation. We see that the Fried length is essentially the size (radius = $D/2$) of an optical system of diameter D that yields a diffraction limited angular size equal to the atmospheric perturbation. In this interpretation with $r_0 = D/2$ we get (for a circular aperture diffraction size) $\theta_{\rm FW(to\,first\,Bessel\,zero)} = 2.44\lambda/D$ while the Kolmogorov theory predicts $\Theta_{\rm FWHM}(\lambda, h) = 0.98\lambda/r_0(\lambda, h) \rightarrow 2 \times 0.98\lambda/D \sim 2\lambda/D$, or essentially the same as the diffraction limited full width for a circular aperture with diameter $D = 2r_0$. The practical implication of this is that we want to keep the sub-aperture diameter D of our (ground based) array to be less than $2r_0$. In general we want the aperture diameter to be significantly less than $2r_0$. For ground based optical systems operating at 0.5 μm for astronomy the measured r_0 on "good nights" is about 10-20 cm. Note that r_0 scales with wavelength as $r_0 \propto \lambda^{6/5}$ so that the Fried length is larger at longer wavelengths (better for us). At $\lambda = 1.06$ μm $r_0 \sim$ 20-40 cm at high altitude sites on "good nights." Atmospheric perturbations during the daytime are expected to be somewhat larger than at night. The bottom line is that we ideally want the sub-aperture size to be about 10 cm or smaller. This drives the system design to small sub-apertures and hence low power per sub-aperture for a given total aperture flux. The alternative to small sub-apertures is to use adaptive optics on every sub-aperture, though this would add significant complexity and cost to the design. In addition, smaller optics are generally lower cost per unit area than larger optics, which also encourages smaller sub-apertures sizes. There is a trade space of first order tip/tilt corrections in each sub-aperture vs sub-aperture size.

As an example, if we use a sub-aperture diameter of 10 cm we get a power of 1 kW per sub-aperture for an assumed aperture flux of 100 kW/m^2 (1 km – 100 GW array) and 10 W per sub-aperture for an aperture flux of 1 kW/m^2 (10 km – 100 GW array). In general smaller sub-apertures may be preferred for a variety of reasons including longer coherence length amplifiers at lower power and the future use of lower cost semiconductor optical amplifiers.

9.2 Strehl Ratio and Perturbations

The Strehl ratio (S) is the ratio of the maximum intensity of a real optical system including all perturbations (optical, structural, atmospheric, etc.) to that of an ideal optical system with no perturbations. For a circular aperture with spherical coordinates (r, θ) the Strehl

 DOI: 10.5281/zenodo.3747263

ratio is:

$$S = \frac{1}{\pi^2}\left|\int_0^1\int_0^{2\pi} re^{ik\psi(r,\theta)}d\theta dr\right|^2 \quad \text{with } 0 \le S \le 1$$

where $\psi(r,\theta)$ is the "aberration function" over the aperture.

Note for the zero aberration case with $\psi(r,\theta) = 0 \rightarrow e^{ik\psi(r,\theta)} = 1$:

$$\int_0^1\int_0^{2\pi} rd\theta dr = \pi \rightarrow S(\psi(r,\theta) = 0) = 1.$$

The aberration function, $\psi(r,\theta)$, has the units of length (error).

When the RMS phase error $\sigma_\phi = k\sigma_\psi <\sim 2$ rad then we can used the extended Marechal approximation:

$$S(D) = e^{-{\sigma_\phi}^2} = e^{-1.03(D/r_0)^{5/3}}$$

since ${\sigma_\phi}^2(D) = 1.03(D/r_0)^{5/3}$.

This now allows us to compute the Strehl ratio for a given system with diameter D and atmospheric perturbation $C_n^2 \rightarrow r_0 \rightarrow \sigma_\phi \rightarrow S$ (see Figure 17).

This approximation works for small to modest perturbations where

$$S(D) = e^{-{\sigma_\phi}^2}$$

gives precisely the same Strehl as the Ruze theory for random optical perturbation of a converntional optical system, and this has been shown to also be the same as the Strehl for random phase perturbations of a phased array where σ_ϕ = standard deviation of the phase error (rad) of an array of sub apertures.

Note that for $D = r_0$ we have $S(D = r_0) = 0.36$. For reference, before the Hubble Space Telescope was fixed with the costar optics the Strehl ratio was about 0.1, while after the costar optics it was close to unity.

Keep in mind that we are more interested in "encircled power" rather than Strehl ratio, as it is the fraction of the power on the reflector. Except for very large mass missions or small arrays, we will essentially never be in the far field of the array, so we will change the focus as the mission increases in distance. Since we do not want the beam flux to be too high on the reflector, we will "defocus" the beam in the early stages of the acceleration phase, and then at L_0 we will come to as tight of a focus as we can and keep the smallest spot possible until we turn off the laser. This implies a much more complex phasing adjustment than simply maximizing the Strehl. Nonetheless, the ability to maximize the Strehl for a given atmospheric perturbation spectrum requires keeping the sub-aperture size sufficiently small as to not increase the spot size (decrease the Strehl and increase the encircled power). If we want high Strehl it is important to keep the sub apertures diameter (D) significantly smaller than r_0, as the Strehl decreases with increasing D:

$S(D = 2r_0) = 0.04$
$S(D = r_0) = 0.36$
$S(D = r_0/2) = 0.72$
$S(D = r_0/3) = 0.85$
$S(D = r_0/4) = 0.90$

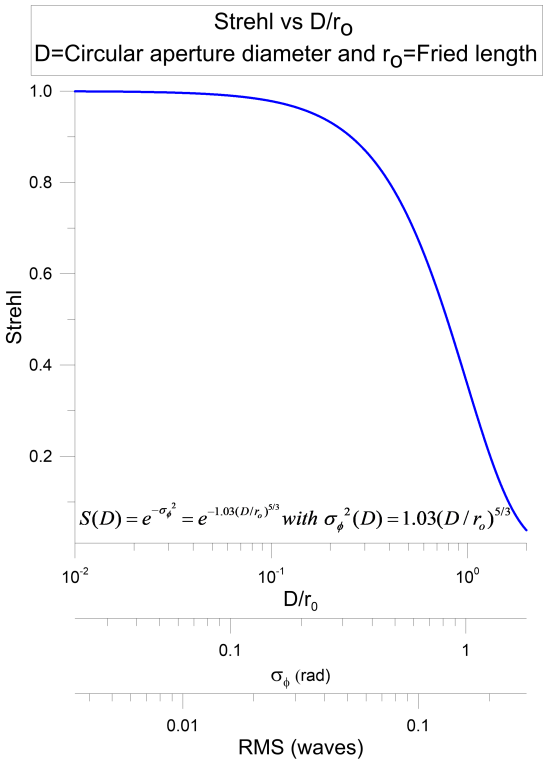

FIGURE 17. *Strehl ratio as a function of aperture size/Fried parameter ratio.*

10 Spacecraft Launch Options

10.1 Spacecraft Ground Launch Option -- Dispensing with the Orbital Dispenser

In theory it is not necessary to launch from an orbital or even airborne platform, but one could start directly from near ground level. In the photon only drive mode such a system could use "tower launch system" to deploy the spacecraft from a suitable height above the array and then use a small portion of the array to start the drive at low power to slowly boost the spacecraft through the atmosphere (see Figure 18). Part of the issue here is to use a small portion of the array and thus maintain a reasonable F# for the tower height. For example, in the case of a wafer scale launch where the mass in the gram scale, we would need 1.5 MW/g to start the (low) acceleration of the spacecraft. In a ground based array case with 100 kW/m^2 aperture flux this would only require about 15 m^2 of the array to be used, or about a 4 m diameter. The tower height for F# = 1 (as an example) would then only need to be 4 meters. It is feasible to go to even lower F# if needed. Such a launch tower could be built at the edge of the array with a rotatable horizontal boom to hold the spacecraft prior to launch. Turning on additional portions of the array would allow for simple "steering" and control of the target vector for the spacecraft, adding flexibility in targeting.

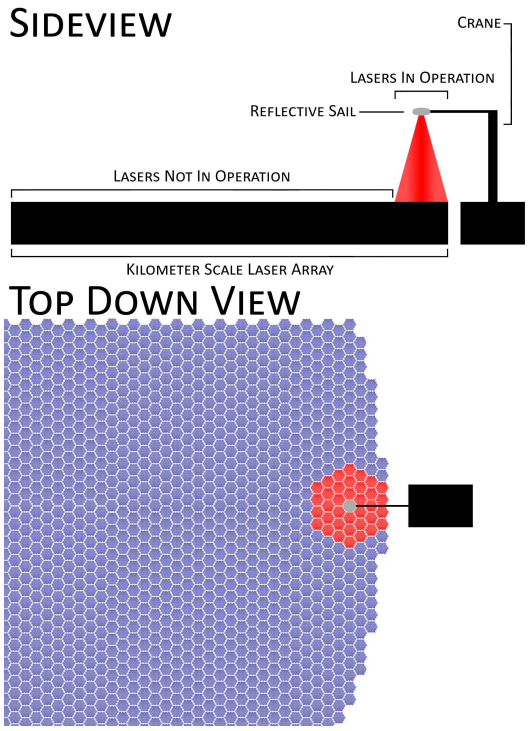

FIGURE 18. *A small portion of the laser array may be used to initiate a ground launch.*

10.2 Drone and Balloon Launch Option

Drones or UAV's can fly to altitudes that allow us to get above a significant portion of the atmosphere and allow for additional launch options (see Figure 19). Drones can fly to altitudes of approximately 30 km in extreme cases, and current technologies are already pushing long duration drones capable of lifting a very large number of small spacecraft. Even low altitude drones that fly below 1 km are of interest, as they allow vastly more flexibility than orbital launchers. This is particularly true when one considers the difficulty of launching spacecraft to a target where alignment of the ground array, orbital launcher and target are required. This alignment is not easy and severely restricts targeting. An additional concern with orbital launchers is their cost and lack of flexibility to allow for new generations of spacecraft, as each new generation of spacecraft will require a new orbital launcher to be deployed. The advantage of an orbital launcher is that it is above the atmosphere and allows complete deployment in a vacuum. In the end a number of tests will be necessary to determine which approach is most applicable and economic.

At the current maximum drone altitude (30 km) the atmosphere has a pressure of about 1% of that at sea level and thus we would be above about 99% of the air. High altitude balloons are another possibility with achieved altitudes of 45 km, but they are not currently able to "station keep" and thus move with the high altitude winds. For launch testing purposes, as well as for atmospheric propagation studies and beacon testing, balloons offer an attractive alternative to orbital launchers.

The advantage of a high altitude platform launch drone or balloon is that the costs are extremely low compared to a space deployment of the spacecraft, even if the array is on the ground. This type of launch is in a 1 g environment and thus we would have to maintain "photon thrust" above 1 g. Power levels in the main beam must be $P_0 > c * m * g/2$ where m is the combined mass of the spacecraft and sail. This requires

 DOI: 10.5281/zenodo.3747263

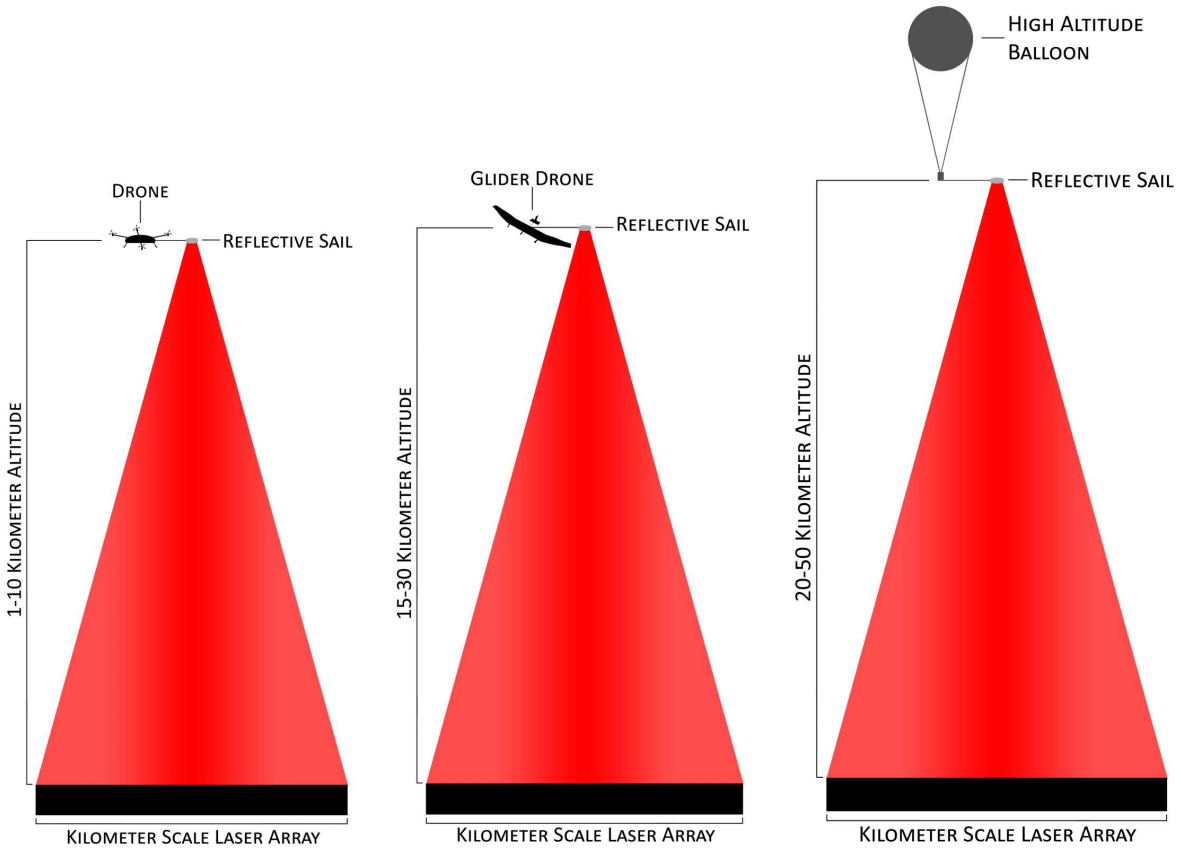

FIGURE 19. *Drones or balloons may be used to carry spacecraft to high altitudes before undergoing photonic acceleration.*

$P_0 > 1.5$ GW/kg or 1.5 MW/g. Hence $P_0 = 1.5$ GW would just "levitate" a 1 kg mass (CubeSat class). But a 1 g mass (combined wafer and sail) would accelerate at about 1000 g's at 1.5 GW. Using a drone at some 10 km is one option as is a balloon at 30+ km. This provides an interesting option for testing. We would need to have $L_0 = dD/2\lambda > z$, where z is the drone/balloon launch altitude above the array. For example, a $d = 100$ m array at $\lambda = 1$ μm and $D = 1$ m sail with a total mass of 1 g (spacecraft + sail) would have $L_0 = 5 \times 10^7$ m, or well above any reasonable upper atmosphere launch vehicle. Even a $d = 1$ m array would have $L_0 = 5 \times 10^5$ m (500 km), again well above any atmospheric launch vehicle. We thus have an option of using a high altitude launch for testing as long as the power is sufficient to levitate the system. **One option is to lower the power level to keep the acceleration and speed in the upper atmosphere low enough to not destroy the sail and then ramp up the power as we exit the atmosphere.** This allows for a series of economical launch tests that are extremely difficult in the lab due to the limited and expensive vacuum pipe needed for extremely high speed testing. The same drone/balloon can carry a series of beacons for atmospheric mitigation and phase testing as well as spacecraft tracking and beam riding tests.

It is possible that this type of launch may be sufficient for full system launches thus removing the need for a space asset for launch IF a ground based laser is used. It would allow for a vastly lower cost to test the system before going to a space launched "mothership" asset. In addition, new spacecraft designs could be quickly implemented for a ground or atmospheric based launcher. This also has significantly increased options for "targeting" in that it allows much more flexibility than a space asset in the case of a ground laser,

due to the complexities of maneuvering a space asset in a "near geo" orbit. Multiple options exist in deployment of the sail as it could be "stowed" during the atmospheric phase and then deployed once out of the atmosphere if needed. There are a number of concerns with atmospheric shear winds that would need to be understood and tested in any such system.

Note that a full size 100 GW array could "ground launch" a 67 kg mass (payload and sail) "spacecraft." This mode could be very useful for LEO, MEO, lunar or outer planet missions where higher mass and lower (nonrelativistic) speeds are required. For the typical sub-elements we are considering for Earth use (approximately 10 cm or less), in the upper atmosphere (approximately 40 km altitude) the spot size produced by a sub-element will be smaller than the sail. Since the full array is highly defocused for this type of high mass ground launch, the overall "beam efficiency" or "fractional power in main lobe" can be near unity as the array during the initial ascent phase does not have to be phase locked in the normal way we have described. A competing effect is the non normal incidence from array sub-elements off the chief ray thus slightly reducing the momentum transfer to the sail. In such a high mass launch scenario, the "spacecraft" would need to start at an altitude roughly equal to the radius of the array. This could be done using a high tower or an aircraft assisted launch.

Using this type of system for an ablative or heat transfer mass ejection engine allows for a wide range of extremely high mass options.

For a similar array on the Moon for example, the same 100 GW array could launch a roughly 400 kg "spacecraft" from the lunar surface using photon momentum transfer only or ablative/heat transfer mass ejection engine launches of extremely high mass. The great advantage of the Moon is the lack of an atmosphere allowing for very high speed launch options.

11 Dual System Shuttle -- Ping Pong Mode

In theory two systems (two photon drivers or one photon driver and a large reflector at the destination) could be used to shuttle a payload back and forth to a destination. In the far future such a system could be used for Earth orbit to the moon, Earth/lunar to Mars, etc. (See Figure 20). In this case the sail reflector is made to be just large enough so that at midway ($\sim$ 0.2-0.5 AU for Mars) the spot size from the array is diffraction limited on it. This reflector size is independent of the payload mass and hence this is **not** an optimized case where sail mass = spacecraft mass. The reflector mass is generally a small fraction of the spacecraft mass for larger mass spacecraft. For example, a 10 km laser array operating at 1.06 μm will have a spot size at 0.5 AU of 15 m. For a 1 μm thick reflector that is square with a size of 20 m the mass would be about 0.4 kg. If perfected, the "ping-pong" mode would allow extremely rapid travel within the solar system.

The time to a distance L where the laser spot is always within the reflector size D is:

$$t_L = (2L/a)^{1/2} = (2Lmc/P_0(1+\varepsilon_r))^{1/2}$$
$$= [2Lc(\xi D^2 h\rho + m_0)/P_0(1+\varepsilon_r)]^{1/2}$$

$$a = P_0(1+\varepsilon_r)/(\xi D^2 h\rho + m_0)c.$$

Peak Speed at distance L is:

$$v_L = a * t_L$$
$$= P_0(1+\varepsilon_r)/(\xi D^2 h\rho + m_0)c$$
$$\times [2Lc(\xi D^2 h\rho + m_0)/P_0(1+\varepsilon_r)]^{1/2}$$
$$= [2LP_0(1+\varepsilon_r)/(\xi D^2 h\rho + m_0)c]^{1/2}.$$

See Figure 21 for plots of t_L and v_L. Reflector size needed to keep main beam inside reflector is:

$$D = 2\lambda a_d L/d.$$

A far future program using the same core technology, but scaled to much higher power, could be used to propel a crewed mission accelerated at 1 g that would get to Mars, including slowing down and orbital insertion, in less than 3 days. However, the power requirements would be vastly higher than what we have outlined for relativistic low mass missions. The power levels required for this would be comparable to the total electrical power that humanity currently uses.

Beamed power ion engine missions - Another option we are currently exploring and funded for is to use

 DOI: 10.5281/zenodo.3747263

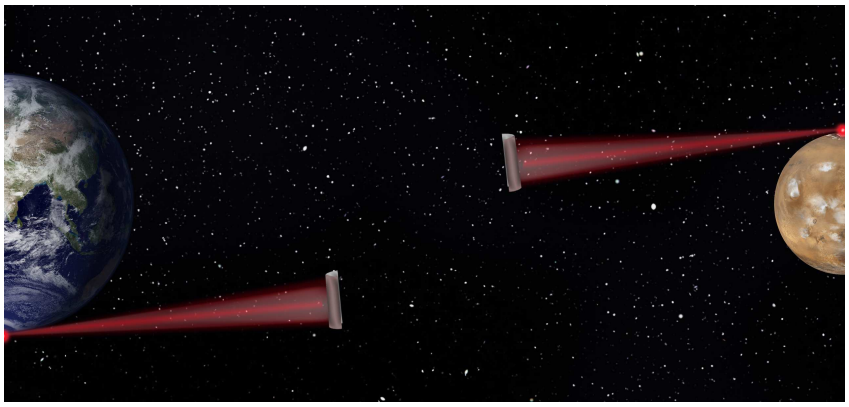

FIGURE 20. *Laser arrays on Earth and Mars operating in "ping pong" mode for rapid travel within the solar system.*

the same core technology to beam power to a spacecraft that is then photoconverted to electricity to drive high performance ion engines. This uses exactly the same laser technology but is much more energy efficient for nonrelativistic high mass missions that are particularly useful inside of our solar system. This is useful for both robotic and crewed missions, including those to Mars, and does not require a system at the destination. Note that this technology cannot achieve relativistic flight and thus cannot be used for interstellar missions.

12 Intermediate Steps and Deployment Strategy

This program represents a long term "roadmap." Along the way there are a number of strategies for both technology development as well as intermediate science goals that should be a part of the longer term effort. One way to begin this discussion is to focus on the current state of the art and understand both the current limitations as well as the ability to leverage existing technologies. Current directed energy systems are all focused on small apertures and modest power for practical reasons. Current aperture sizes are less than 1 m with powers approaching 100 kW CW. For most current DE applications there is little current interest in pushing to large apertures, though somewhat higher powers are desired. It is instructive to compare the aperture flux for a DE-STAR class 4 system, which is about 1 kW/m^2. This is small by comparison to existing DE systems which have an aperture flux of about 100 kW/m^2. This is encouraging, as our needs are long baseline with modest aperture (as opposed to target) flux. Since the system we propose is a modular system with identical elements we can specify an aperture flux $\Psi_{\rm ap}$ (W/m^2) with $P_{\rm optical} = \Psi_{\rm ap} A = \Psi_{\rm ap}\xi_{\rm array} d^2$ and power in the main beam $P_0 = \varepsilon_{\rm beam} P_{\rm optical} = \varepsilon_{\rm beam}\Psi_{\rm ap}\xi_{\rm array} d^2$.

The laser array has area $A = \xi_{\rm array} d^2$, where d is the array size as defined above. Note we use the same symbol ξ for the sail geometry factor but $\xi_{\rm array}$ for the laser array geometry factor.

We can write the max (optimized case) speed with continued illumination as:

$$\begin{aligned} v_{\max -\infty} &= \left(\frac{P_0(1+\varepsilon_r)d}{c\lambda\alpha_d}\right)^{1/2} (\xi h\rho m_0)^{-1/4} \\ &= \left(\frac{\varepsilon_{\rm beam}\Psi_{\rm ap}\xi_{\rm array} d^2(1+\varepsilon_r)d}{c\lambda\alpha_d}\right)^{1/2} \\ &\quad \times (\xi h\rho m_0)^{-1/4} \\ &= d^{3/2}\Psi_{\rm ap}^{1/2}\left(\frac{\varepsilon_{\rm beam}\xi_{\rm array}(1+\varepsilon_r)}{c\lambda\alpha_d}\right)^{1/2} \\ &\quad \times (\xi h\rho m_0)^{-1/4} \end{aligned}$$

Note the scaling of the speed with the array size:

$$v_{\max -\infty} \propto d^{3/2}\Psi_{\rm ap}^{1/2}$$

Hence for every increase by a factor of 10 in array size (and hence a factor of 100 increase in power and array area) the speed increases by $10^{3/2} = (1000)^{1/2} \sim 31.6$, or increasing the array size by a factor of 100 increases the speed by a factor of 1000 for a constant aperture flux

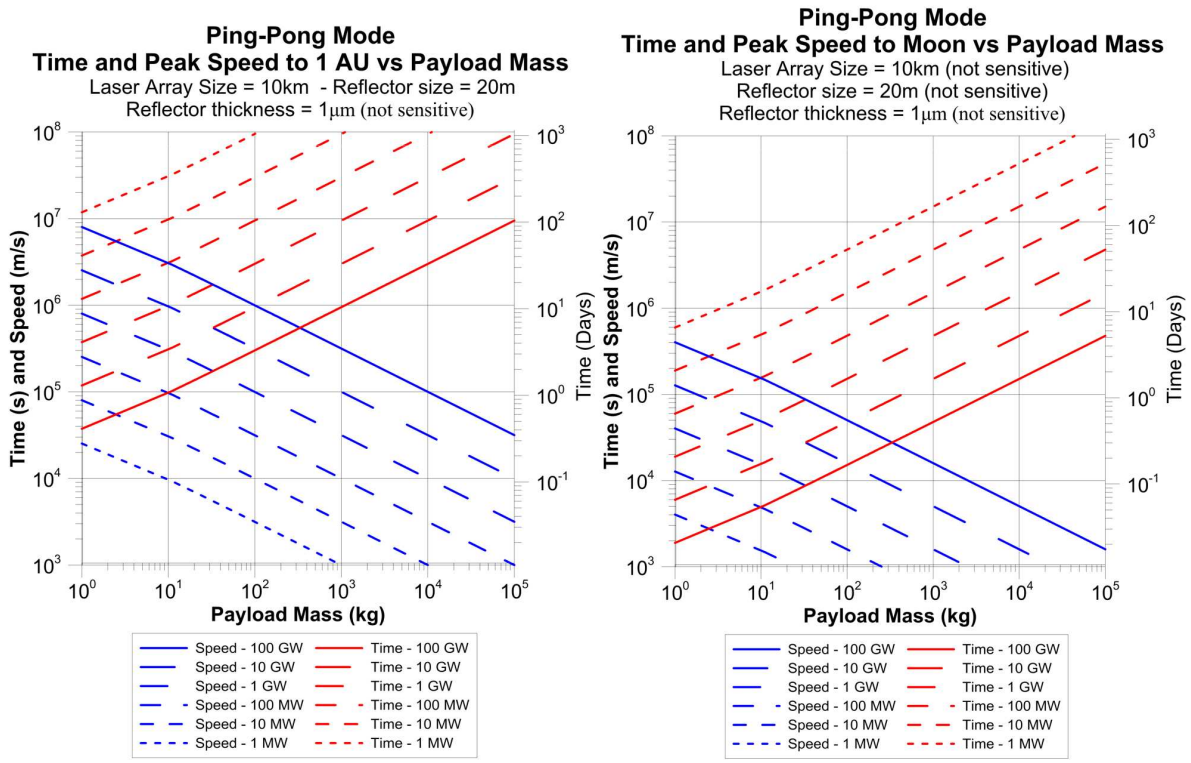

FIGURE 21. *t_L and v_L as a function of payload mass.*

$\Psi_{\rm ap}$.

The speed rises rapidly as we increase the size of the array assuming each sub-element has a constant aperture flux. This is equivalent to building the array from a set of identical sub-elements, each of which has aperture flux $\Psi_{\rm ap}$. One building strategy is to do precisely that; start with a defined aperture sub-element and build increasingly large arrays based on this sub-element. In addition to a technical approach, this is also a logical economic approach as the prototype sub-elements can be built with increasing cost effectiveness with both increased technology improvements in manufacturing (and likely changing core technologies) as well as an economy of scale. In addition there are a number of feedback and feed forward loops that need to be designed, and the smaller arrays with lower total power are less challenging in feedback/forward time scales and time of flight issues.

We show speed versus array size 1 m to 1 km for aperture flux densities of 1, 10 and 100 kW/m^2 for payloads of 1 g (wafer scale) and 1 kg ("CubeSat scale") with sails of 0.1 and 1 micron thicknesses in Figure 22. Even thinner sails can be imagined. For example a 10 nm (0.01 micron) sail (about 100 atoms thick) may be possible someday. Such a sail would increase the speed in the nonrelativistic limit by a factor of $10^{1/4}$, or about 1.8, compared to that of a 0.1 μm sail. We thus have a wide field of mission space as we proceed along the technology development roadmap. The fastest chemical propulsion (not including gravitational dives and orbital assists) barely exceeds 10 km/s, or about 0.00004c, with Voyager now going at 17 km/s as mentioned earlier. Even at 0.01% of c (0.0001c) we exceed chemical propulsion systems, and this occurs with relatively modest arrays along the roadmap to relativistic flight. We thus enable a variety of missions within our solar system along the roadmap to interstellar flight. This synergy between technological development in the roadmap and the execution of numerous solar system missions and beyond is one of the many reasons to pursue the core technology presented here. It is also one of the great strengths of this program in that progress in both technology and missions go "hand in hand" as a part of the overall roadmap, so it is never an "all or

 DOI: 10.5281/zenodo.3747263

nothing" approach to exploration.

13 Payload Sizes

Once a suitable laser photon driver is built the payloads can be any size from miniature relativistic probes, such as the wafer scale one for interstellar flight we have discussed, to large spacecraft capable of transporting humans in the solar system. A single photon driver can be used to launch sequentially, or in parallel, any number of spacecraft, and thus the system enables and is amortized over a large mission space. As the speed scales as a mild function of payload mass in the optimized case ($v \sim m_0^{-1/4}$) there is a wide set of options in mission planning. Increasing the mass by a factor of 10 reduces the speed by a factor of about 1.8, increasing the mass by a factor of 100 reduces speed by about 3.2, and increasing the mass by 10^4 reduces speed by a factor of 10. This allows for mission possibilities not simply focused on relativistic wafer scale systems, but extending to extremely large payloads for interplanetary needs. **Adding in the beamed power mode for driving ion, ablation, and thermal engines enables an even wider parameter space**. See Figure 23 for plots of spacecraft speed as a function of array size for heavier payloads.

14 Logical Spacecraft Mass Approach

It is far easier to work with larger mass payloads due to the lower accelerations, slower response times and easier and more capable spacecraft design. For a given power the acceleration (and control complexity) is inversely proportional to the mass and for a given array size and power the speed goes as $m^{-1/4}$. We propose a logical "roadmap" would be to focus on larger payload masses and interplanetary mission (for example 1-10 kg) as the laser array is developed. We are currently in a NASA Phase II for studies and prototyping of such systems using both direct photon drive and beamed power to ion engine drive.

15 Ultra Thin Wafer Scale Electronics

To reach the goal of a gram scale spacecraft, low mass and high component density electronics are crucial. Most semiconductor wafers used in large scale digital and analog electronics have thicknesses of about 300-500 microns. This is primarily done for handling issues. The thickness needed for the devices themselves is dependent on the device type, but can be extremely shallow with some devices taking less than 20 nm depth. Large wafers can easily be made much thinner (terrestrial solar PV is already less than 100 microns for example). With reactive ion etching (as one example), a "waffle crate" structure can make the wafer very low mass with the surface thickness at less than 1 micron as needed. Recent work at IBM has shown simple techniques for "peeloff" fabrication with sub-micron thicknesses. There has been little need for ultra thinned wafers since the driver is low cost production rather than mass minimization, but large advances are easily possible in this area. As one example, a "waffle crate" structure with an effective surface thickness of 1 micron would have a mass of about 2.3 g/m^2. Current devices made with 22 nm fabrication techniques have approximately 17 million transistors per square mm with about 5 billion devices per CPU (size $\sim$ 1-2 cm). With the push to 3D processing it is estimated that within 10 years the density of transistors could exceed 100 billion/cm^2. While one micron sounds very thin, in the realm of 3D processing it is already 100 layers with 10 nm spacing. It is not unreasonable to assume that within 20 years the equivalent CPU will easily exceed 1 trillion devices and thus a 1 gram ultra thinned 1 micron thick wafer could exceed 1 Peta (10^{15}) transistors. This is about 1 million times the computational power of a modern high end (i7 equivalent) laptop. We can thus trade power needs, functionality and wafer mass and will have a wide range of options.

16 The Road to Monoatomic Electronics and Reflectors

In addition to the push for 3D processing there is also a strong push to the limits of atomic engineering, with monatomic systems being one goal. As an example the thickness of a monatomic graphene sheet is about 0.35 nm, with a C-C spacing of 0.14 nm, tensile strength estimated to be about 130 GPa, and a Young's modulus of 1-3 TPa, and thus a strength that is estimated to be several hundred times that of the highest strength steels. Assuming a density of 2.3 g/cc this would give an areal density of about 0.8 mg/m^2. This is MUCH lower than

DOI: 10.5281/zenodo.3747263

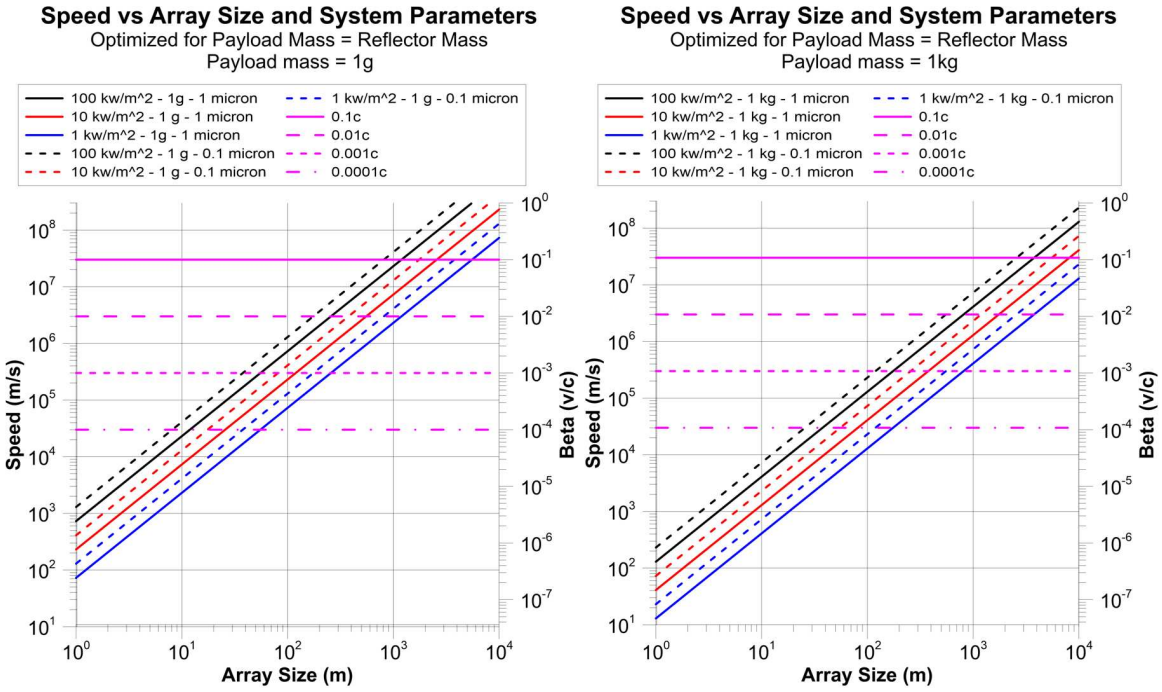

FIGURE 22. ***Left:*** *Speed and Beta vs array size from 1 m to 10 km for 1, 10 and 100 kW/*m^2 *aperture flux for a 1 g (wafer scale) payload with a 0.1 and 1 micron thick sail material. Array is square. Lines of interest for 0.01% c (30 km/s), 0.1% c (300 km/s), 1% c (3000 km/s) and 10% c (30,000 km/s) are shown for reference. The best chemical propulsion systems (without gravity and orbital assist) are limited to about 10 km/s.* ***Right:*** *Same but for a 1 kg payload.*

the current state of the art in solar reflectors, which is a few microns thick or a few g/m^2. Thus monatomic graphene would be more than 1000 times lower areal mass than current reflectors.

Using graphene to make both electronics and reflectors would have significant consequences for interstellar flight. The possibility of making vastly lower areal density reflectors would allow much higher speed for the same power, or reduced power and array size for the same speed. As discussed above, the speed for an optimal system (sail = payload mass) scales with thickness h as:

$$v_{\max -\infty} = \left(\frac{2P_0 d}{c\lambda\alpha_d}\right)^{1/2} (\xi h \rho m_0)^{-1/4}.$$

Reducing the reflector thickness from 1 micron to 0.35 nm (single layer graphene) would increase the speed by $(1000/0.35)^{1/4} \sim 7.4$ in the nonrelativistic limit. Such a reduction in reflector thickness would also allow the product of photon driver power and size ($P_0 d$) to be reduced by a factor of $(1000/0.35)^{1/2} \sim 53$. In addition to its use in reflectors, graphene could also play an increasingly important role in electronics. Such changes would be extremely useful and are something to continue to keep in mind as progress in materials develops. A number of issues are important, including the radiation resistance and the erosion from interstellar gas (mostly protons) and dust collisions. Recent work indicates that graphene is relatively radiation resistant.

17 Wafer Scale Spacecraft

While photonic propulsion can be used to propel any mass of spacecraft, the lower the mass, the faster the speed as discussed above. As a part of our NASA Phase I and II programs, we have studied very low mass spacecraft with masses typically at the gram level. While it seems far fetched to image an entire spacecraft on a wafer, it is quite feasible for certain classes of spacecraft. From imaging to spectroscopy, and even life detection as well as propulsion, power, and laser communication, these capabilities can all be integrated onto a

 DOI: 10.5281/zenodo.3747263

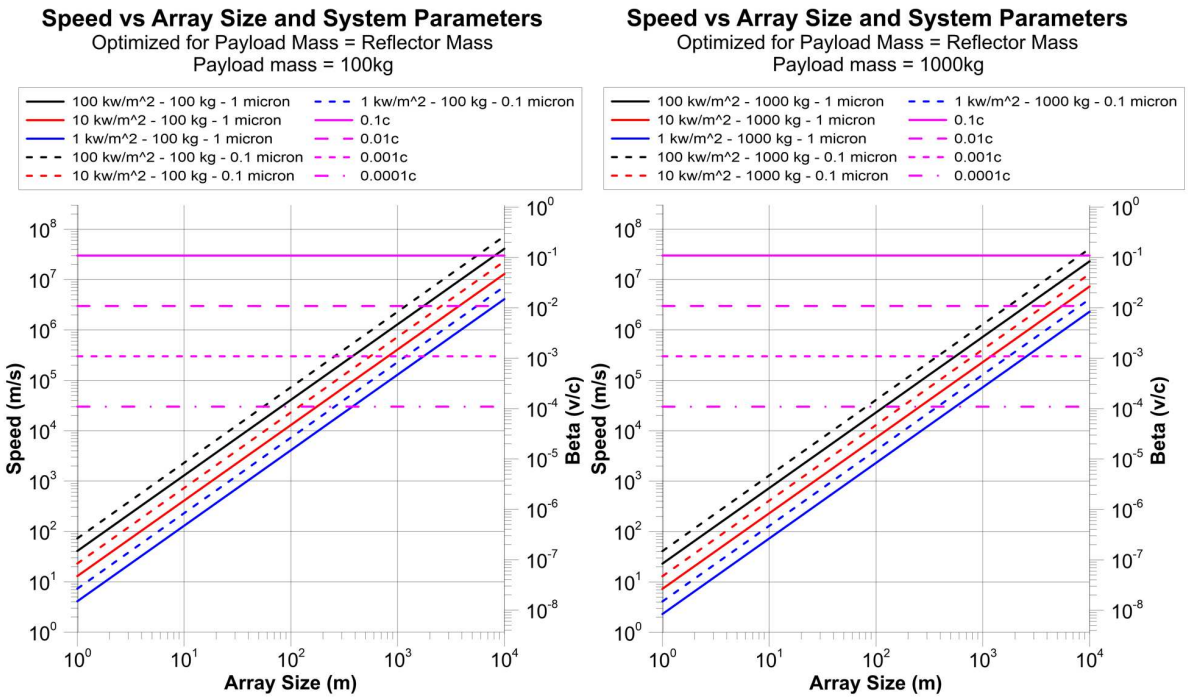

FIGURE 23. *Same as Figure 22 but with 100 and 1000 kg payloads.*

wafer either directly or via hybridization. While Si is easiest to work with, many other semiconductors are viable, including III-V for photonic integrated circuits (PIC) as well as future carbon (graphene) based semiconductors. Considering the advances in "cell phone technology" as one obvious comparison, modern processors have well over one billion devices on a single cm scale portion of a wafer with full wafers currently accommodating well over a trillion devices. Such an approach allows for easily replicated, extremely reliable and very low cost approaches to production.

While the public has been fixated on our 10 cm and below wafers as relativistic spacecraft (see Figure 24), it is feasible to explore ultra thin and large area wafer scale spacecraft in the meter class. These options offer the advantage of both low mass and extreme quantities of devices (Petascale level) as well as greatly enhanced area for PV power and laser (or radio for short range applications) communications, allowing much higher data rates. This is clearly an area of extremely rapid growth propelled by other factors in the semiconductor industry which we can leverage.

17.1 Large Diameter Low Mass Wafer Scale Spacecraft

With the largest current Si wafers near 0.5 m in diameter, it is conceivable that meter diameter wafers could be produced in the next 20 years. With Si having density of 2.3 g/cc, at the current size of 0.5 m this would give a 1 micron thick wafer a mass of 0.45 g. If 1 m diameter wafers became available this would increase the mass by 4x, or 1.8 g assuming a 1 micron thickness. Thinning further to 0.55 microns would give a mass of 1 g. If we assume a 30 nm nominal depth requirement per device layer this would give about 30 device layers per micron. For a 0.55 micron thick Si wafer with 30 nm layers this gives about 18 layers. If we scale from the current 14 nm to 5 nm feature scale that is expected in the near future we would get about 200 million devices/mm^2 or 200 trillion devices per m^2 per 30 nm layer. For a hypothetical 1 m diameter round 1 g wafer thinned to 0.55 microns with 30 nm layers this would yield 3 Peta devices, or more than the largest current supercomputer. There is no current need for this many devices on our wafer scale spacecraft, but it shows the potential for the future.

DOI: 10.5281/zenodo.3747263

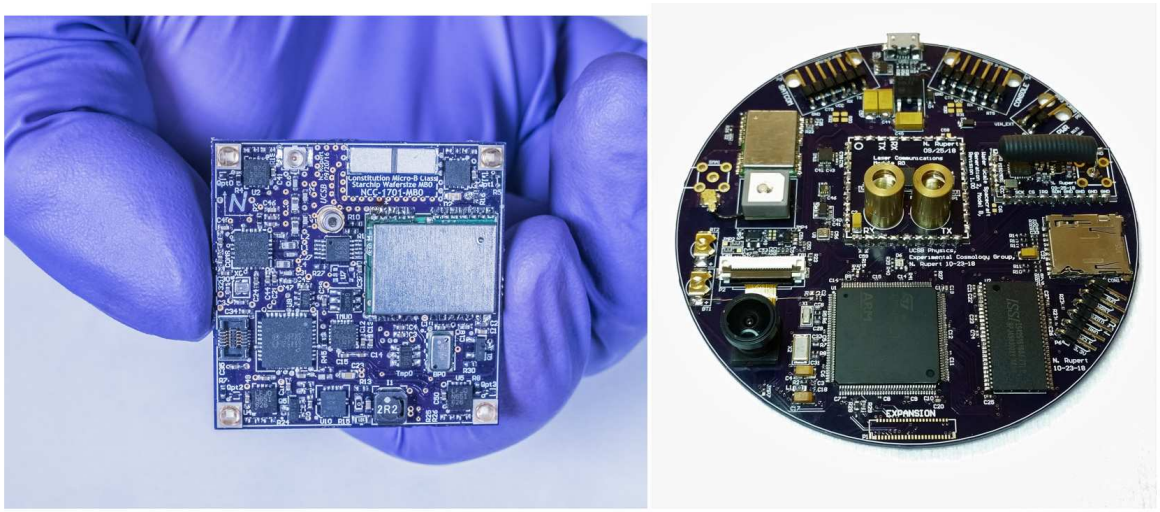

FIGURE 24. ***Left:*** *Third generation UCSB "wafer scale spacecraft" with laser communications and multiple additional sensors.* ***Right:*** *Fourth generation WSS with bi-directional laser comm., radio link , GPS, imaging, attitude determination and numerous additional sensors for LEO and planetary applications.*

17.2 Large Area Photovoltaics

One significant advantage of large diameter wafers is the ability to deposit thin film PV, allowing much greater power upon arrival. At 1 AU in an Earth/Sun-like system the solar insolation is 1400 W/m^2, yielding about 400 $\mathrm{W_{elec}}/\mathrm{m}^2$ at 30% efficiency. Advances in the next 10-50 years could yield 50% or greater efficiency allowing, 700 $\mathrm{W_{elec}}/\mathrm{m}^2$.

One caution is the need to explore the radiation resistance of various device structures and ways to mitigate damage, such as the thermal annealing that was recently suggested and tested.

These advances allow us to ponder two interesting options:

1) Extremely thin (micron and sub micron) large diameter wafers with enormous capability.

2) Smaller diameter lower mass wafers allowing great speed or lower power, smaller diameter laser arrays.

In general there would be a range of spacecraft from the very low mass, extremely high speed ones to larger mass and more capable ones. Since the time scale in both photonics and electronics is exponential we can look forward to enormous advances in this area. **In the time scale of a single mission to the nearest stars our technology will continue to advance with rapid changes in wafer scale spacecraft. This will not be a static field.**

17.3 The Sail and the Spacecraft as One Unit

One option to explore is the use of an integrated sail/spacecraft, where the large diameter wafer is itself also the reflector, with one side being a photonic crystal for reflection and the other side the "active" side. Another possibility is to have two wafers, possibly with different materials, that are bonded and possibly inflated, to make a hybrid sail and wafer.

18 Wafer Level Thrusters for Attitude Control and Maneuvering

Photon thrusters and miniature ion engine thrusters may be used for wafer scale spacecraft maneuvering and are worth comparing in depth. Both are compatible with wafer scale technology and each offers advantages and disadvantages.

 DOI: 10.5281/zenodo.3747263

18.1 Photon Thrusters

Photon thrusters using small lasers or narrow angular emission LED's offer conversion efficiency from electricity to photons of above 50%, with some devices now at 80%. In addition, any "heat" from inefficiency is also ultimately emitted as photons, so a properly designed system can be nearly 100% efficient, though we have to be careful to include "directional efficiency or solid angle effects." Photons thrusters are extremely simple, reliable, and lend themselves to virtually any orientation. They can also be operated in CW or short pulse modes and possibly be incorporated into portions of the laser comm system. Another type of photon thruster is a direct heat rejection photon thruster, using excess heat (from the RTG for example) as gated heat pipes. This is more complex but would allow the thermal heat to bypass the electrical conversion process, which is relatively low efficiency, and hence have nearly 100% efficiency BUT with many complications added. The force F for a photon thruster in transmission is $F(\mathrm{N}) = P_\gamma(\mathrm{W})/c$ or about 3.3 nN/W assuming a perfectly collimated beam (zero divergence). The total momentum transfer "Δp" from the photon thruster is simply $\Delta p_\gamma(\mathrm{N\,s}) = F_\gamma(\mathrm{N})\tau = P_\gamma(\mathrm{W})\tau/c = E(\mathrm{J})/c$, where τ is the time the photon thrusters are on. The photon thrust case is simple as the spacecraft mass m_0 (bare spacecraft and sail mass combined) does not change. To be precise, the spacecraft mass does change due to energy loss (and hence mass) carried away by the photons, but this rest mass change is generally extremely small. We can compare the photon thrust force to an ion engine (electrospray or any variant). For an ion engine the thrust is $F_{\mathrm{ion}}(\mathrm{N}) = 2P_{\mathrm{ion}}(\mathrm{W})/gI_{sp}$. This assumes zero divergence for the ions. In this case the "ion engine" is just a placeholder for any mass ejection engine. Note that P_γ and P_{ion} is the actual power in the photons/ions and not the electrical input power. We note it is generally much harder to produce a well collimated beam of ions compared to photons, and hence an ion beam is degraded in effective thrust more than photon thrusters for a given power level, but since $c >> gI_{sp}/2$ **ion engines produce much more thrust per unit power than photon thrusters**. The limitation is of course that ion beams, like all mass ejection engines, need fuel, which adds mass and limits supply, while photon thrusters have no fuel and hence no intrinsic limit in this area. Still, for many applications ion thrusters are advantageous for maneuvering.

18.2 Mass Ejection Thrusters

Miniature ion engines are emerging, which may allow a realistic option for even wafer scale systems. For example, single tip electrospray thrusters are compatible with wafer scale fabrication and could be effectively used for maneuvering during the cruise phase. With I_{sp} in the 2000-4000 s range these would allow significantly more attitude and transverse maneuver controls than our baseline photon thrusters for the same power level. The amount of ejection mass needed is small compared to the system mass, and thus they are an attractive alternative, as they are vastly more energy efficient for the same momentum transfer (ratio of I_{sp}).

19 Multi Tasking and Multimodal Operation

A photon driver can simultaneously track many targets up to the number of beam sub-elements. This means multiple missions can be simultaneously engaged, as well as multimodal operation (different tasks). This not only gives the system extreme flexibility, but allows for amortization and efficient use of the resource.

20 Ground Vs Space Deployment of Laser Photon Driver

It would be far simpler and less expensive if we could deploy the main photon driver on the ground rather than in space. In [4] we discuss the issue of ground, airborne and space deployment options for our related technology work on DE planetary defense [7, 4]. The primary concern for ground deployment is the perturbations (seeing) of the atmosphere. With typical "seeing" at "good" mountain top sites of a bit better than 1 arc second ($\sim$ 5 microrad) this is far from the required 0.1 nrad. Even the best adaptive optics systems fall far short of this. With the upcoming 30 m class telescopes we hope to be able to get to decent Strehl ratios with multi AO systems but at much larger diffraction limited values than we need. Ground based interferometry in the visible is done with 10 m class telescopes with modest success, which is encouraging. The two Keck telescopes on Mauna Kea are about 85 m apart, while the VLT's can be up to 200 m apart and the NPOI (Navy Precision Optical Interferometer) has a 440 m baseline. This is also encouraging. The key will

DOI: 10.5281/zenodo.3747263

be to produce high fractional encircled energy (Strehl). The optimization of where to deploy in space is also a part of a longer term analysis (LEO, GEO, lunar, L2, etc.). These are not only very cost-sensitive optimizations, but suitability for maintenance is also a significant factor. **During the development and test phase of the roadmap we will explore the limits of ground based deployment to better quantify this.** Smaller laser arrays, say 0.01-1 km, should be built for ground use before going to space. Ground deployment does offer much lower cost and the option of much higher areal power density to offset the reduced array size. **This will also help us understand ground deployment of the PAT (Phased Array Telescope) mode.** In addition, the ground based solution for a PAT is complicated by the atmospheric air glow and non thermal processes, such as OH lines in particular [8]. Weather is also an issue as are water vapor fluctuations [9, 6]. For the spacecraft to ground laser communications, an onboard local oscillator to tune the laser could be commanded from the ground using the laser array to transmit a command to the wafer. The atmospheric emission is mitigated by use of a very narrow linewidth laser for communications since the data rates are low. Uplinking commands is feasible (modulo TOF) using the laser array to transmit. Once the spacecraft is far away the TOF will be complicated and tracking and beacon locking will be challenging in all cases, whether in space or on the ground. In order to minimize backgrounds for reception it is highly desirable to fully synthesize the received beam as discussed above. This requires knowledge of the location of the spacecraft and knowledge of both the astrometry and ephemeris at (sub) nrad levels. This is not trivial. Ground deployment should be explored before the space option primarily due to the dramatic reduction in cost and ease of maintenance and expansion.

20.1 Limitation of Ground Based Array Deployment

One key complication of a ground based deployment is the limited target and the limited payload classes as well as laser communication data reception. This problem arises from two sources. One is that for a given deployment latitude the availability of targets on the sky is limited by the fact that atmospheric perturbations become worse the further away the target is from zenith. This will tend to restrict the target options to launch windows when the target declination is within a limited acceptable zenith angle. If this is combined with an orbital payload launch dispenser (OPLD), then the launch windows become even more restrictive. Combining this with the Earth's rotation and tracking requirements places further limitations on launches. Overall this will tend to restrict payloads to lower masses to meet the limited illumination times consistent with all of the above issues. Adding in weather variability will further confine the launch windows. For example, if one of the targets of interest is the Alpha Centauri system, which has an approximate declination angle of δ = -63 deg, then only deployment latitudes comparable to -63 deg would be acceptable. The acceptable zenith angle for operation would have to be determined for each site, but one could imagine that a zenith angle of about 30 degrees would be possible. This would then open up sites with latitudes of -33 to -90 degrees.

20.2 Polar Deployment

The polar regions, in particular the S. Pole area, are deployment options that should be explored. The lack of aircraft and birds and lesser number of satellite assets, improved atmospheric properties, remoteness and fewer people and animals prone to laser backscatter are all reasons to consider polar deployment. Tracking during the acceleration phase is also simplified (being azimuthal) and much longer illumination times become possible compared to mid latitude sites. In addition, 50% of the year is dark allowing for greatly improved data reception. However, there are a number of downsides to polar deployment. The remoteness increases the cost and the long nights make maintenance difficult. Data reception will be much more difficult during the 50% of the year that is daytime. The polar regions also have auroras and line emissions that must be considered. Sites such as the South Pole and the "domes" A, C, and F are good candidates to explore. The S. Pole is particularly interesting given the significant infrastructure that is already present. A detailed cost/benefit analysis would have to be done to decide on which ground based sites are desired. Multiple ground based sites are also an option, though this will increase total cost.

20.3 Space Based Deployment Options

Space based deployment is the preferred long term solution in terms of superior targeting options, in particular for larger mass payloads which require longer illumination time. The lack of atmosphere is a major advantage

 DOI: 10.5281/zenodo.3747263

as well, though the clear disadvantage is the vastly increased cost of deployment. While a sun synchronous LEO orbit is the lowest cost solution, there are superior longer term solutions including lunar deployment that offer advantage. For example, the back side of the moon or the lunar polar regions would be excellent sites if a lunar infrastructure were to be deployed. The slow rotation of the moon is also advantageous. Any space based solution would be part of an evolving long term program.

21 TRL Advancement

There are a wide variety of TRL levels in this system. Some parts, such as laser amplifiers, have high TRL in the lab but not in space while others, such as long baseline phase synthesis, have low overall TRL. There are also specific space deployment TRL issues such as radiation induced color centers in fibers, radiation shielding, thermal management in orbit, and others that will need to be addressed as part of a full program for eventual large scale space deployment. These issues are not critical to solve now but will be in the longer term. Some can be tested in the laboratory (beam line radiation tests for example) and some can be tested in small orbital tests (flying laser amplifiers on the ISS without external beam emission for example). Some of the unique space deployment TRL issues also depend on the long term deployment strategy option chosen (LEO, GEO lunar).

22 Cost Comparison to Recent and Past NASA Programs

Any realistic directed energy propulsion system to reach relativistic speeds will be expensive. It is useful to compare to some of the larger NASA programs to some of the system cost estimates. A critical difference is that the cost of the R&D phase of the DE program we are discussing, that will likely last over several decades, will be coupled to an exponential technology which is unlike any past NASA program. The system will also be driven by other market factors (telecom, high speed photonic interfaces in commercial electronics, etc.) and other forces will push the "DE market," as well as DoD DE programs. Our current estimates are based on both realistic cost expectations from existing DE and optics technologies as well as the assumed exponential growth in photonics. The latter, as discussed, is already going on and will almost certainly continue for reasons that have nothing to do with DE driven propulsion. For example the current worldwide photonics market is nearing 180 B$/yr (2016 USD) with Si photonics expected to exceed 1 T$ by 2022 with annual growth rates of approximately 20%. **These numbers dwarf the entire current chemical launch industry and show the "engine" upon which a DE program would be propelled economically.**

For historical reference we note the Apollo program, built upon a very large and expensive infrastructure that was primarily DoD in its origins (ICBM's), cost (NASA side only) about 200 B$ in 2016 USD. The Shuttle program cost about 210 B$ in 2010 USD. US cost of the ISS was about 75 M$ in 2014 USD. The JWST will cost in total close to 10 B$ in the end.

Another critical factor is that if a DE launch were to be space based (as opposed to ground based) then the launch and space deployment costs will likely completely dominate the program. Ground based DE, as discussed, is only feasible IF we can overcome the atmospheric perturbations.

23 Other Benefits

As we outline in our papers, the same basic system can be used for many purposes, including both stand-on and stand-off planetary defense from virtually all threats with rapid response, orbital debris mitigation, orbital boosting from LEO to GEO, future ground to LEO laser assisted launchers, standoff composition analysis of distant objects (asteroids for example) through molecular line absorption, active illumination (LIDAR) of asteroids and other solar system bodies, and beamed power to distant spacecraft, among others. **This technology will enable transformative options that are not possible now and allows us to go far beyond our existing chemical propulsion systems with profound implications for the future** [4, 2, 10, 11, 12].

24 The Path Forward

This is a long term program and as such needs to progress in a logical fashion. Being scalable, the system lends itself to a "roadmap." In addition, as the atmosphere is relatively transparent at 1064 nm, ground testing of large systems becomes possible (though it

imposes severe restrictions) and thus testing prior to space based deployment is possible. We propose a logical phase of 1) Laboratory scale R&D and testing, 2) Ground based testing of increasingly capable systems, 3) Sub-orbital testing on balloons of small scale systems in near space-like conditions and 4) Orbital testing of systems from CubeSat and ISS based (as a possible example) to future large orbital structures to lunar siting. The options for space deployment are vast, and once the technology is mastered the possibilities are virtually endless and applications will not be limited to a single system.

25 Conclusions

It is now feasible to seriously discuss, plan and execute a program to use directed energy to propel spacecraft to relativistic speeds, allowing the possibility of realistic interstellar flights for the first time as well as use the same technology for many other applications, including beamed power modes. There has been a dramatic change in the practical possibilities of using directed energy brought about by a revolution in photonics that is on an exponential rise in capability and an exponential drop in cost. While photonic propulsion has been spoken about for a very long time, it has largely been confined to the realm of dreams and science fiction. This has now changed to the point where a serious program can begin to enable a future no longer constrained by low speed chemical and ion propulsion. We outline a roadmap to that future with a logical series of steps and milestones. One that is modular and scalable to any sized system. The same system has many other applications and spinoffs, and this will greatly aid in the cost amortization. While the roadmap to the future of directed energy propulsion is extremely challenging, it is nonetheless possible for a feasible roadmap to begin. The difficulties are many but the rewards and long term consequences are not only profound but will be transformative for humanity.

Acknowledgements

We gratefully acknowledge funding from NASA NIAC Phase I NNX15AL91G and NASA NIAC Phase II NNX16AL32G as part of the NASA Starlight program and the NASA California Space Grant NASA NNX10AT93H as well as a generous gift from the Emmett and Gladys W. Technology fund in support of this research. PML gratefully acknowledges support from the Breakthrough Foundation as part of the Starshot program. Portions of this paper are from an upcoming book entitled "The Path" by P. Lubin 2020.

Website Resources

Resources are available on our website that include papers, images and videos as well as a photon propulsion calculator that implement both the nonrelativistic as well as relativistic equations for mission analysis, see `https://www.deepspace.ucsb.edu/projects/starlight`.

References

[1] Hughes, G., Lubin, P., Bible, J. *et al.* (2013). DE-STAR: phased-array laser technology for planetary defense and other scientific purposes (Keynote Paper). In *Proc. of SPIE Vol. 8876, 88760J*.

[2] Lubin, P., Hughes, G., Bible, J. *et al.* (2013). Directed energy planetary defense (Plenary Paper). In *Proc. of SPIE Vol. 8876, 887602*.

[3] Hughes, G., Lubin, P., O'Neill, H. *et al.* (2016). DE-STAR: phased-array laser technology for planetary defense and exploration. *Advances in Space Research - Special Edition: Asteroids and Space Debris*.

[4] Lubin, P. and Hughes, G. (2015). invited chapter on "Directed Energy for Planetary Defense". *Springer Verlag*.

[5] Kulkarni, N. and Lubin, P. (2016). Relativistic Directed Energy Propelled Spacecraft. *In preparation*.

[6] Suen, J., Fang, M., and Lubin, P. (2015). Global Distribution of Water Vapor and Cloud Cover - Sites for High performance THz Applications. *IEEE Trans. THz Science and Technology*, **4**:86.

[7] Hughes, G., Lubin, P., Griswold, J. *et al.* (2014). Optical modeling for a laser phased-array directed energy system (Invited Paper). In *Proc. of SPIE Vol. 9226*.

 DOI: 10.5281/zenodo.3747263

[8] Lubin, P. (2016). The Search For Directed Intelligence. *REACH*.

[9] Suen, J., Fang, M., Denny, S. *et al.* (2015). Modeling of Terabit Geostationary Terahertz Satellite Links from Globally Dry Locations. *IEEE Trans. THz Science and Technology*, **5**.

[10] Lubin, P., Hughes, G., Bible, J. *et al.* (2016). Toward directed energy planetary defense. *Optical Engineering*, **53**.

[11] Riley, J., Lubin, P., Hughes, G. *et al.* (2014). Directed energy active illumination for near-Earth object detection. In *Proc. of SPIE Vol. 9226*.

[12] Zhang, Q., Walsh, K., Melis, C. *et al.* (2015). Orbital Simulations of Laser-Propelled Spacecraft. In *Proceedings of Nanophotonics and Macrophotonics for Space Environments, SPIE*.

DOI: 10.5281/zenodo.3747263